NASA Technical Memorandum 106367

Effect of Wind Tunnel Acoustic Modes on Linear Oscillating Cascade Aerodynamics

Daniel H. Buffum
Lewis Research Center
Cleveland, Ohio

and

Sanford Fleeter
Purdue University
West Lafayette, Indiana

Prepared for the
38th ASME International Gas Turbine and Aeroengine Congress and Exposition
sponsored by the American Society of Mechanical Engineers
Cincinnati, Ohio, May 24–27, 1993

NASA

Effect of Wind Tunnel Acoustic Modes on Linear Oscillating Cascade Aerodynamics

Daniel H. Buffum
National Aeronautics and Space Administration
Lewis Research Center
Cleveland, Ohio

Sanford Fleeter
Thermal Sciences and Propulsion Center
School of Mechanical Engineering
Purdue University
West Lafayette, Indiana

ABSTRACT

The aerodynamics of a biconvex airfoil cascade oscillating in torsion is investigated using the unsteady aerodynamic influence coefficient technique. For subsonic flow and reduced frequencies as large as 0.9, airfoil surface unsteady pressures resulting from oscillation of one of the airfoils are measured using flush-mounted high-frequency-response pressure transducers. The influence coefficient data are examined in detail and then used to predict the unsteady aerodynamics of a cascade oscillating at various interblade phase angles. These results are correlated with experimental data obtained in the traveling-wave mode of oscillation and linearized analysis predictions. It is found that the unsteady pressure disturbances created by an oscillating airfoil excite wind tunnel acoustic modes which have detrimental effects on the experimental data. Acoustic treatment is proposed to rectify this problem.

NOMENCLATURE

C	airfoil chord
C_p	unsteady pressure coefficient, $p_1/(\rho_{in}V_{in}^2\alpha_1)$
$\hat{C}_p^n$	unsteady pressure influence coefficient due to oscillation of n-th airfoil
$\overline{C_p}$	steady pressure coefficient, $(p_{in}-p_0)/(\rho_{in}V_{in}^2)$
k	reduced frequency, $\omega C/V_{in}$
M	Mach number
n	relative position of oscillating airfoil
p_j	j-th harmonic of airfoil surface static pressure
p_{in}	mean inlet static pressure
S	airfoil spacing
t	time
V_{in}	inlet velocity magnitude
x	airfoil chordwise coordinate
α_j	j-th harmonic of incidence angle
β	interblade phase angle
γ	stagger angle
ΔC_p	unsteady pressure difference coefficient
ρ_{in}	inlet density
ϕ	phase of unsteady pressure coefficient
ω	airfoil oscillation frequency (radians/second)

INTRODUCTION

Aerodynamically-induced vibration of the blading in gas turbine engines is an ongoing problem which affects both the development cost of new engines and the reliability and maintenance costs of existing engines. Accurate analysis tools could reduce these costs significantly, hence the development of advanced aerodynamic analyses for oscillating cascaded airfoils is of current research interest. Oscillating cascade experiments play a key role in the development of these analyses, providing data used to both evaluate existing analyses and provide direction for advanced modeling efforts.

A review of previous oscillating cascade investigations reveals there are, in general, few data available for cascaded airfoils driven to oscillate simultaneously. Focusing on subsonic and transonic flows for axial compressor geometries, there are several noteworthy publications. Davies and Whitehead (1984) performed experiments in an annular oscillating cascade in subsonic through supersonic flow regimes, but the measurements were limited to unsteady aerodynamic moments. Kobayashi (1989) has made detailed blade surface pressure measurements in an annular oscillating cascade at high subsonic and supersonic inlet conditions. Large pressure fluctuations occurred due to shock wave motion and cascade instability was noted over a wide range of conditions. Unsteady pressure measurements have been made at the NASA Lewis Research Center in a linear cascade which was oscillating in a traveling-wave mode (Buffum and Fleeter, 1991). In some instances, it was found that unsteady pressure disturbances reflected by the wind tunnel walls interfered with the cascade unsteady aerodynamics.

The lack of oscillating cascade data is due to the inherent complexity of the experiments. First, oscillating cascades are expensive to build, traditionally requiring a drive system capable of oscillating the airfoils simultaneously in traveling-wave modes for various interblade phase angles at realistic values of the reduced frequency. Second, because the measurements must be obtained not only for each steady flow condition and reduced frequency, but also over a range of interblade phase angles, the experiments can be quite time consuming. As a result, data are typically obtained only for several interblade phase angles.

An alternative to the traveling-wave mode of oscillation is the unsteady aerodynamic influence coefficient technique. Assuming the unsteady disturbances are small, as in a typical flutter stability problem, only one airfoil in the cascade is oscillated, with the resulting unsteady pressures measured on the oscillating airfoil and its stationary neighbors. Through summation of these influence coefficient data, the unsteady aerodynamics of an equivalent cascade with all airfoils oscillating at any specified interblade phase angle may be predicted.

Figure 1 depicts a two-dimensional finite cascade representation of a blade row. For a given mean flow field and reduced frequency of oscillation, and assuming small unsteady disturbances, the cascade unsteady aerodynamics may be expressed as linearly combined influence coefficients which can be determined experimentally or analytically. Consider a finite airfoil cascade with $2N+1$ airfoils executing constant amplitude harmonic oscillations with a constant interblade phase angle β. The airfoil surface unsteady pressure, expressed as a pressure coefficient $C_p(x,y,\beta)$ acting at a point on the reference airfoil (airfoil 0 in Figure 1), can be expressed as a Fourier series

$$C_p(x,y,\beta) = \sum_{n=-N}^{N} \hat{C}_p^n(x,y) e^{in\beta} \qquad (1)$$

where $\hat{C}_p^n(x,y)$ is the complex-valued unsteady aerodynamic influence coefficient. This influence coefficient defines the unsteady pressure coefficient developed on the reference airfoil at the point (x,y) due to the motion of airfoil n.

Mathematical models for an infinite cascade of airfoils oscillating with a specified interblade phase angle can also be used to determine these unsteady aerodynamic influence coefficients. For this case, the influence coefficients are determined by inversion of Equation 1:

$$\hat{C}_p^n(x,y) = \frac{1}{2\pi} \int_{-\pi}^{\pi} C_p(x,y,\beta) e^{-in\beta} d\beta. \tag{2}$$

Analytically-determined unsteady aerodynamic influence coefficients can thus be found from oscillating cascade analyses by integrating predicted values of C_p over the complete interblade phase angle interval per Equation 2. Substituting these influence coefficients into Equation 1 then enables analytical predictions for a finite number of airfoils oscillating in an infinite cascade to be determined.

If this technique is valid, the most important advantage is that the drive system must oscillate only one airfoil, reducing the complexity and cost of the experimental facility. In addition, as already mentioned, the influence coefficients may be used to predict the cascade unsteady aerodynamics for any interblade phase angle, although these predictions are theoretically suspect in the vicinity of acoustic resonances (Buffum and Fleeter, 1990a). An added advantage is the physical insight gained by knowing the values of the various influence coefficients and therefore the impact that the oscillations of airfoil n will have on the stability of the reference airfoil.

Several experimental investigations have been directed at validation of this technique through correlation of unsteady aerodynamic influence coefficient results with corresponding data acquired with all airfoils oscillating at specified interblade phase angles. Hanamura et al. (1980) found good results for flow in a water channel, but this is insufficient to validate the technique for compressible flow. Davies and Whitehead (1984) performed such experiments at high subsonic inlet conditions and reduced frequencies to 0.21, but there was considerable scatter in the traveling-wave mode data. In supersonic inflow experiments, Széchényi (1983), the summation of influence coefficients has been compared to data for a linear cascade with two airfoils oscillating, but the scope of the experiments was very limited. Bölcs et al. (1989) reported very good results for this technique in an annular turbine cascade with mean exit flow fields ranging from subsonic to supersonic and reduced frequencies as large as 0.42. Buffum and Fleeter (1990a) reported good results using this method, but further analysis now indicates some shortcomings in the data which are similar to those discussed in this paper.

Of the investigations mentioned above, only that of Bölcs et al. was conclusive regarding the influence coefficient technique. However, as those experiments were conducted in an annular cascade, it would be rash to conclude that this technique is also valid for use in a linear cascade. While circumferential pressure disturbances are free to propagate around the annulus of an annular cascade, disturbances will be constrained by the wind tunnel walls in a linear cascade, possibly resulting in detrimental effects on the cascade unsteady aerodynamics. In fact, in traveling-wave mode experiments, Buffum and Fleeter (1993) found that reflection of unsteady pressure disturbances off the wind tunnel walls interfered with the linear cascade unsteady

aerodynamics for some interblade phase angles. Thus it is important to thoroughly investigate the validity of this technique in a linear cascade environment.

In the present study, the unsteady aerodynamic influence coefficient technique is investigated in a low solidity linear oscillating cascade. The cascade solidity, 0.65, was chosen to be representative of an advanced propeller model which fluttered during wind tunnel tests (Mehmed et al., 1982). For an inlet Mach number of 0.55, the torsion mode biconvex airfoil oscillating cascade aerodynamics are investigated for reduced frequencies as high as 0.90. To help ascertain the validity of the influence coefficient technique, correlation of the influence coefficient results is made with data obtained for all of the airfoils oscillating at various interblade phase angles and the predictions of a linearized oscillating cascade analysis.

OSCILLATING CASCADE FACILITY

The NASA Lewis Transonic Oscillating Cascade, Figure 2, combines a linear cascade wind tunnel capable of inlet flow approaching Mach one with a high-speed airfoil drive system which imparts torsion-mode oscillations to the cascaded airfoils at specified interblade phase angles and realistically high reduced frequency values.

Air drawn from the atmosphere passes through a smooth contraction inlet section into a constant area rectangular test section of 9.78 cm span which measures 58.6 cm along the stagger line. Upstream of the test section, suction is applied through perforated walls to reduce the boundary layer thickness. Tailboards are used to adjust the cascade exit region static pressure and also form bleed scoops which further reduce upper and lower wall boundary layer effects. Downstream of the test section, the air is expanded through a diffuser into an exhaust header. The exhaust system, part of a central air facility at Lewis, maintains a 30 kPa pressure downstream of the flow control valves. The cascade inlet and the airfoil angles may be adjusted to obtain a wide range of incidence and stagger angle combinations.

The facility features a high-speed mechanism which may drive any or all of the airfoils in controlled torsional oscillations. Stainless steel barrel cams, each having a six cycle sinusoidal groove machined into its periphery, are mounted on a common rotating shaft driven by a 74.6 kW electric motor. A cam follower assembly, consisting of a titanium alloy connecting arm with a stainless steel button on one end, is joined on the other end to an airfoil trunnion. The button fits into the cam groove, thus coupling the airfoil to the camshaft. Lubrication of the cam/follower assembly is provided by an oil bath. The amplitude of the torsional airfoil motion is 1.2 degrees as dictated by the cam and follower geometry. The drive system is configured for oscillations at a chosen interblade phase angle by fixing the cams at the required relative positions on the shaft. A reduced frequency of 0.90 is achieved at 0.55 inlet Mach number with an oscillation frequency of 350 Hz. For more information on the experimental facility, see Buffum and Fleeter (1990b).

AIRFOILS AND INSTRUMENTATION

The airfoil and cascade geometry is summarized in Table 1. Four uncambered, 7.6% thick biconvex airfoils were used to create a low solidity (C/S=0.65) cascade. The stagger angle was 45 degrees and the airfoils oscillated about the midchord.

Airfoils instrumented with static pressure taps were used to measure the airfoil surface steady pressure distributions. There were sixteen chordwise measurement locations, with a higher

density in the leading edge region used to capture the larger gradients there. Rows of sidewall static pressure taps located upstream and downstream of the cascaded airfoils were used to determine the mean inlet and exit pressures.

Flush-mounted high-frequency-response Kulite pressure transducers were used to measure the unsteady surface pressures on the oscillating airfoils. Two airfoils were instrumented, each having six transducers mounted symmetrically about the midchord on one airfoil surface. These transducers, having active sensor diameters of 1.3% of the airfoil chord, were epoxied into milled slots and potted in room-temperature-vulcanizing rubber for isolation from airfoil strain. A thin coating of rubber was also used to fair the transducer surface into the airfoil contour.

From static and dynamic calibrations, the pressure transducers were found to be highly linear in response over the frequency and pressure ranges of interest. However, the pressure transducers may produce undesirable signals as a consequence of the airfoil motion. This effect was quantified by oscillating the instrumented airfoils under no-flow conditions. The response of each transducer was found to be a linear function of the airfoil acceleration, implying that the acoustic response, which varies with the airfoil velocity magnitude, was dominated by the acceleration response. These calibration data were used to correct the oscillating airfoil pressure data for acceleration effects.

The time-dependent position of the reference oscillating airfoil was determined by a capacitance-type proximity sensor which produces a voltage proportional to the air gap between it and an adjacent object. This sensor was positioned to face a six cycle sinusoidally-shaped cam mounted on the airfoil drive camshaft so as to be in phase with the reference airfoil motion.

DATA ACQUISITION AND ANALYSIS

Conventional instrumentation was used to quantify the steady flow field. An average of the upstream sidewall static pressures along with the atmospheric (total) pressure were used to calculate the inlet Mach number. Steady flow airfoil surface static pressures were calculated from an average of approximately 100 samples in time at each tap. The steady pressure coefficient at a point (x,y) on the airfoil surface is defined in Equation 3.

$$\bar{C}_p(x,y) = \frac{p_{in} - p_0(x,y)}{\rho_{in} V_{in}^2} \tag{3}$$

p_{in} is the mean inlet static pressure, p_0 is the mean airfoil surface static pressure, and ρ_{in} V_{in} are the inlet values of density and velocity.

Unsteady signals were recorded on magnetic tape for post-experiment processing. During tape playback, the signals were simultaneously digitized at rates sufficient to capture at least three harmonics of the oscillation frequency, with 32,768 samples taken per channel. Each channel of data was divided into contiguous blocks, each block typically with 2048 samples, and then Fourier decomposed to determine the first harmonic of each block of data. The first harmonic pressure of each block was referenced to the airfoil motion by subtracting from it the phase of the first harmonic motion signal of the same block. Once all of the blocks from a channel were decomposed in this manner, the first harmonic block results were averaged and the complex-valued acceleration response was subtracted vectorally. Statistical analysis of the block results was used to estimate uncertainties for the average first harmonic values.

The motion of an oscillating airfoil is defined by the change in the incidence angle with time: $\alpha(t) = \alpha_0 + \alpha_1 \cos(\omega t)$ where α_0 is the mean incidence angle, α_1 is the torsional oscillation amplitude and ω is the frequency.

The complex-valued unsteady pressure coefficient is defined as

$$C_p(x,y) = \frac{p_1(x,y)}{\rho_{in} V_{in}^2 \alpha_1}. \tag{4}$$

p_1 is the first harmonic airfoil surface static pressure. The dynamic pressure difference coefficient is the difference between the lower (y^-) and upper (y^+) surface unsteady pressure coefficients:

$$\Delta C_p(x) = C_p(x,y^-) - C_p(x,y^+). \tag{5}$$

RESULTS

The experimental influence coefficient technique is investigated in a linear oscillating cascade. For a mean inlet Mach number of 0.55 and 2 degrees mean incidence, the airfoil surface steady pressure coefficient distributions are presented first. Then the unsteady aerodynamic influence coefficients are presented, with special attention given to the effect of the relative position of the oscillating airfoil, the effect of reduced frequency, and convergence of the influence coefficient series. Finally, the influence coefficient predictions are correlated with data for all airfoils oscillating and linearized analysis predictions.

STEADY STATE AERODYNAMICS

For a linear cascade to be a valid simulation of a turbomachine blade row, the cascade must exhibit good passage-to-passage periodicity for the steady flow field. In Figure 3, steady pressure coefficient data are presented for the center cascade passage and the two adjacent passages. Good cascade periodicity is apparent, with the only significant differences found at the leading edge of the airfoil upper surface.

The upper surface pressure coefficient distribution peaks near the leading edge with a corresponding maximum Mach number of 0.74. At the lower surface peak of $\overline{C}_p = -0.25$, the Mach number is 0.39. There is negligible loading beyond 50% of chord. Using the method of Kline and McClintock (1953), a 95% confidence interval of ±0.003 is estimated for these pressure coefficients. The exit region mean static pressure divided by the inlet total pressure was 0.825.

UNSTEADY AERODYNAMICS

Influence Coefficient Technique

Chordwise distributions of the first harmonic pressure influence coefficients on the individual surfaces of the position 0 instrumented airfoil are presented for the oscillating airfoil in the five relative positions defined by n=-2 through n=2.+ But first, sample time-dependent pressure

+By varying the location of the oscillating airfoil in the cascade, five influence coefficients were obtained using the four-airfoil cascade; schematic diagrams included with the experimental results presented later in this paper will clarify the various cascade configurations.

signals are presented along with the resulting pressure spectra in Figure 4. These results illustrate the typical dominance of the first harmonic that was found in the signals. 95% confidence intervals of ±5% in magnitude and ±4 degrees in phase were estimated for the mean value of the first harmonic pressure coefficients.

Dynamic Periodicity. To investigate the dynamic periodicity of the cascade, self-induced unsteady pressure data were obtained for the two airfoil locations surrounding the cascade center passage. That is, an instrumented airfoil was oscillated in position A of Figure 5 with the other airfoils fixed. Then an instrumented airfoil was oscillated in position B with the other airfoils fixed. The resulting unsteady pressure coefficients $\hat{C}_p^0$ are presented for k=0.90. Ideally, the unsteady pressure data for these two positions would be identical, but this is not the case for these data. On the airfoil lower surface, the magnitude periodicity is good except at 60 and 75% of chord, and the phase periodicity also varies with position, being good at 12, 75 and 88% of chord but having significant differences otherwise. The upper surface magnitude periodicity is not particularly good at any measurement location, although the phase periodicity is good except for the 12 and 40% of chord locations. For the rest of this paper, data obtained from the airfoil surfaces defining the center passage of the cascade will be used for $\hat{C}_p^0$.

There are several possible causes of the shortcomings in the periodicity data. One would be a lack of periodicity in the mean flow field coupling with the unsteady perturbations to produce aperiodic behavior in the unsteady flow. Since the steady flow periodicity was found to be very good, this is not likely to be a problem.

It is more likely that the lack of dynamic periodicity was caused by acoustic waves created by the oscillating airfoils interacting with the wind tunnel walls and the wind tunnel flow field. One form of interaction would be reflection of waves propagating away from the cascade along the axis of the wind tunnel by nonuniformities in the flow, for example gradients found at the wind tunnel inlet and also at the diffuser section. At the nonuniformities, some fraction of the incident acoustic energy would be reflected back toward the cascade while the rest continues to travel away from the cascade.

Propagating and decaying acoustic waves will be created by an airfoil oscillating airfoil in a wind tunnel. Since the decaying waves decay exponentially with distance from the airfoil, only propagating acoustic modes are likely to reach either the inlet or diffuser with significant energy. The modal cutoff frequencies, which determine whether or not a mode will propagate, are given in the Appendix for a rigid rectangular duct of width A' and height B' with uniform axial flow at Mach number M. For waves propagating either upstream or downstream without attenuation, the requirement for the frequency of oscillation is

$$\omega > \omega_{lm} = a_0 \sqrt{(1-M^2)\left[\left(\frac{l\pi}{A'}\right)^2 + \left(\frac{m\pi}{B'}\right)^2\right]} \tag{6}$$

for integer values of l and m. Thus the (l=0,m=0) modes always propagate. For the present wind tunnel geometry (A'=9.60 cm and B'=41.4 cm), the (0,1) mode has the lowest non-trivial cutoff frequencies, 337 Hz. Only for the highest reduced frequency, 0.90 (345 Hz oscillation frequency), will a (0,1) mode propagate, and even then only in the upstream direction. However,

since the (0,0) mode will propagate at all frequencies, the potential always exists for undesirable reflections at the inlet and diffuser sections.

Only some portion of the acoustic energy created by the oscillating airfoil will feed into the propagating modes, and it remains to be seen whether this portion is significant. And the amount of this energy that will be reflected is also unknown. Thus it is difficult to determine whether wave reflections at the inlet and diffuser sections had significant effects on the measurements.

A more direct form of interaction occurs when acoustic waves created by the oscillating airfoil reflect off the wind tunnel walls back toward the cascade. The zero-normal-velocity condition which these rigid walls impose result in reflection of incident acoustic waves and formation of the duct acoustic modes. For a given geometry, the resulting mode shapes depend upon the location of the excitation source, i.e., the position of the oscillating airfoil. Therefore positions A and B of the oscillating airfoil will excite the various modes differently, and only if the resulting acoustic modes are of negligible amplitude relative to the unsteady pressure on the oscillating airfoil will periodic data be expected. Whether this effect is more or less significant than the previously mentioned effects due to flow field nonuniformities is unknown.

Effect of Relative Position of Oscillating Airfoil. To investigate the effect of the oscillating airfoil relative position on the reference airfoil unsteady pressure distribution, first harmonic pressure influence coefficient data are presented for the five relative positions of the oscillating airfoil. For 0.40 reduced frequency, the influence coefficients $\hat{C}_p^n$ are presented for the airfoil lower surface in Figure 6. In the accompanying schematic, each symbol corresponds to the effect of oscillation of the indicated airfoil on the reference instrumented airfoil.

For the lower surface data, the self-induced unsteady pressures $\left|\hat{C}_p^0\right|$ are dominant, attaining a maximum near the leading edge then tending toward zero at the trailing edge. The unsteady pressure magnitude distribution due to airfoil -1 oscillations, the airfoil adjacent to the reference airfoil lower surface, also peaks near the leading edge. As expected, airfoil 1 oscillations cause smaller amplitudes along the forward half of the reference airfoil lower surface, but, unexpectedly, $\left|\hat{C}_p^1\right|$ is slightly larger than $\left|\hat{C}_p^{-1}\right|$ along the aft half. The n=2 and n=-2 magnitudes are quite small, illustrating the expected decrease in unsteady pressure magnitude with distance from the oscillating airfoil.

Lower surface phase angle data are strong functions of the oscillating airfoil position but, for any one value of n, change little with chordwise position. The n=0 phase changes from a small phase lag at 12% of chord to a small phase lead at 60 and 75% of chord. For n=-1 and n=-2, the phase data are roughly out-of-phase, while the n=1 and n=2 phases are closer to being in-phase with the airfoil motion.

For the airfoil upper surface, Figure 7, the self-induced unsteady pressures are dominant over the first 50% of chord. The other unsteady pressures are generally small. Decreasing values of $\left|\hat{C}_p^n\right|$ with distance from the oscillating airfoil are apparent when n=1 and n=2, but when the airfoils upstream of the instrumented airfoil, n=-1 and n=-2, are oscillating, values of $\left|\hat{C}_p^{-2}\right|$, although small, are larger than $\left|\hat{C}_p^{-1}\right|$ in the midchord region. The n=0 unsteady pressure fluctuations are approximately out-of-phase relative to the airfoil motion while airfoil 1

oscillations result in in-phase unsteady pressures. The rest of the unsteady pressures tend to lag the motion by varying amounts.

Effect of Reduced Frequency. To clarify the effect of reduced frequency, the unsteady pressure influence coefficients $\hat{C}_p^n$ are presented individually for each value of n for two reduced frequencies, k=0.40 and k=0.90. Starting with the oscillating airfoil unsteady pressure coefficient distribution, Figure 8, it is shown that the larger amplitudes generally occur at the larger reduced frequency except near the leading edge on the upper surface. For k=0.90, the lower surface amplitudes at a given chordwise location are larger than those for the upper surface. In contrast, for k=0.40, the amplitudes for the two surfaces tend to be equal. Reduced frequency affects the phase distribution on the upper surface somewhat but does not affect the lower surface phase.

Unsteady pressures resulting from oscillation of the airfoil in relative position 1 are shown in Figure 9. A schematic of the cascade as it was configured to obtain these data is also shown - the solid lines above and below the cascade airfoils designate the wind tunnel walls. The unsteady pressure magnitudes at either reduced frequency are nearly constant with chordwise position and equal for each of the two surfaces. The magnitude increases with reduced frequency, k=0.90 having nearly twice the magnitude as k=0.40. For either value of reduced frequency, the phases of the upper and lower surface unsteady pressure are about the same along the aft half of the airfoil. Forward of there, the phase distributions diverge with the lower surface lagging the upper surface. The lower surface phase variation is roughly linear.

Similar trends occur for $\hat{C}_p^2$, Figure 10. For either value of k, the unsteady pressure magnitude distributions vary little with chordwise position and are nearly equal for the two surfaces. The higher reduced frequency data have significantly larger magnitudes. For either value of k, the phase distributions are nearly equal beyond the midchord but diverge over the forward half of the airfoil, with the lower surface lagging the upper surface. The lower surface phases vary in approximately a linear manner.

That the magnitudes of $\hat{C}_p^n$ in Figures 9 and 10 are constant with chordwise position and equal for the two airfoil surfaces suggests that these unsteady pressure distributions are mainly due to planar (mode (0,0)) acoustic waves. Under ideal conditions, such as an acoustic wave propagating upstream past a flat plate aligned with a uniform mean flow, the amplitude of the resulting unsteady pressure on the flat plate would be constant and the phase would vary linearly with chordwise position and have a positive slope. The lower surface phase data approximate this condition, having a fairly linear phase change with chord and positive slope.

There are other characteristics of these data which are consistent with an upstream-traveling acoustic wave. Near the trailing edge, the lower and upper surface phases are equal. The phase distributions for the two surfaces remain approximately equal over the aft half of the airfoil, where steady pressure distributions (and hence Mach number distributions) for the two surfaces are nearly equal. The phase distributions diverge along the airfoil forward half, with the lower surface having larger positive slope, indicating a larger upstream propagation velocity or phase velocity along the lower surface - this is expected because the mean flow velocities are smaller on the lower surface than the upper surface. But the negative slope of the phase distribution found on the upper surface near the leading edge is inconsistent with an upstream-traveling wave. On the whole, however, the upstream-traveling acoustic waves dominate the $\hat{C}_p^1$ and $\hat{C}_p^2$ distributions.

The k=0.90 data from Figures 9 and 10 are cross-plotted in Figure 11 to show that, for the same value of k, $\left|\hat{C}_p^2\right| = \left|\hat{C}_p^1\right|$. This is clearly a wind tunnel effect; without the wind tunnel walls to reflect acoustic waves, $\left|\hat{C}_p^2\right|$ would surely be less than $\left|\hat{C}_p^1\right|$ as a result of the increased distance from the source of the unsteadiness. For the phase data, dashed lines are included to indicate the theoretical phase variation due to an upstream-traveling acoustic wave which is assumed to have the same phase as the 88% of chord, lower surface data for n=1. The theory is in good agreement with the phase data on the lower surface for both n=1 and n=2.

The main effect of oscillating the airfoil in relative position -1 is a peak in the unsteady pressure magnitude near the leading edge on the adjacent, lower surface of the instrumented airfoil, Figure 12. Upper surface magnitudes are very small except near the leading edge. Contrary to the trend for n>0 of larger magnitudes for higher reduced frequencies, the magnitudes on the lower surface are slightly larger for the lower reduced frequency. Phase distributions for the upper surface are quite similar for the two reduced frequencies, both with the phase at 12% of chord leading the phase at 88% of chord by about 150 degrees and having reasonably linear variation with chordwise position. There are large differences due to reduced frequency in the phase distributions on the lower surface: the k=0.40 data remain constant with chord while the k=0.90 data vary greatly with position. There is no clear evidence of a downstream-traveling acoustic wave in the data, most likely because of the sudden change in the duct geometry at the diffuser located immediately downstream of the cascade (Figure 2).

Figure 13 presents $\hat{C}_p^{-2}$. The larger magnitude data occur at the higher reduced frequency. A more significant finding is that the unsteady pressure magnitudes are larger on the airfoil upper surface. Referring to the accompanying cascade schematic, it is seen that the instrumented airfoil upper surface is adjacent to a wind tunnel wall. Pressure waves which were reflected off the wind tunnel wall toward the instrumented airfoil upper surface probably caused the larger pressures there. The phase distributions generally change little with position and are approximately out-of-phase. As in the $\hat{C}_p^{-1}$ data, a downstream-traveling acoustic wave is not apparent.

Summation of Influence Coefficients

Summation of the experimentally-determined influence coefficients to determine the unsteady pressure difference coefficient ΔC_p is depicted in Figures 14 and 15 for the limit of summation in Equation 1, N, varying from 0 to 2 and k=0.90. Thus N=0 corresponds to the self-induced unsteady aerodynamic response. For both values of the interblade phase angle, 0 and 180 degrees, the ΔC_p series is rapidly convergent. Only the oscillations of the reference airfoil and its two immediate neighbors have a significant effect on the resulting dynamic pressure difference coefficients.

In contrast, the series for the unsteady pressure coefficient C_p is not necessarily convergent. For example, Figures 16 and 17 demonstrate summation of the lower surface pressure coefficients for the same conditions as Figures 14 and 15, respectively. In both of these cases, the series are not convergent over the range for which data are available: the phase is rapidly varying with N for $\beta = 0^o$ while the magnitude is not converging for $\beta = 180^o$. This is mainly due to the relatively large magnitudes of $\hat{C}_p^n$ which do not diminish for increasing, positive values of n. The series for the unsteady pressure difference coefficient is convergent despite this because the pressures on the two surfaces largely cancel when the pressure difference is taken. This is evident

from the data in Figures 9 and 10, where the complex individual surface values of $\hat{C}_p^n$ are approximately equal for n=1 or n=2 so that $\Delta\hat{C}_p^1$ and $\Delta\hat{C}_p^2$ are quite small.

Since the amplitudes of $\hat{C}_p^1$ and $\hat{C}_p^2$ increase with reduced frequency, lowering the reduced frequency should result in a C_p series with better convergence properties. This effect is shown in Figures 18 and 19, where a reduction in k to 0.20 while keeping the same Mach number and interblade phase angle results in good convergence for the airfoil lower surface unsteady pressure coefficient.

Correlation of Data

Unsteady pressure difference coefficients obtained via summation of the experimental influence coefficients are now correlated with predictions and with experimental data obtained for oscillation of the airfoils in several traveling-wave modes. The reduced frequency is 0.64 and the interblade phase angles range from -90 to 180 degrees. Summation of the experimental influence coefficient data makes use of all of the available experimental data, that is, N=2 in Equation 1. These data are correlated with the predictions of a computer program published by Whitehead (1987) which is based on the analysis of Smith (1972). The assumptions of inviscid, isentropic, subsonic flow through an infinite cascade of flat plate airfoils are made. The analysis also assumes that the airfoils are at zero mean incidence, and that the airfoil oscillations create small unsteady disturbances to the uniform mean flow. Predictions obtained from Smith's analysis via the influence coefficient technique are also presented for N=2.

As mentioned in the Introduction, the wind tunnel walls have been found to adversely affect some experiments in which all of the airfoils were oscillating simultaneously (Buffum and Fleeter, 1993). For the interblade phase angle values 0, 45, 90 and 180 degrees, the cascade dynamic periodicity was found to be poor, thus the unsteady pressures obtained at these conditions are not reliable and will not be used for correlation purposes.

As shown in Figures 20 through 25, the experimental influence coefficient results and the analytical predictions are generally in good agreement. In addition, where reliable experimental data exist for traveling-wave mode oscillation of the airfoils, $\beta = -45^o$ and -90^o, these data are in good agreement with the experimental influence coefficient results and the analytical predictions. The only significant differences occur at $\beta = 90^o$, Figure 23, where the analytical predictions for the magnitude are offset to larger values than the experimental influence coefficient results. In general, the analyses tend to predict slightly larger magnitudes than the experimental influence coefficient results. For values of β ranging from 0 to 90^o, the analytical phase predictions tend to lead the experimental influence coefficient results by a small amount. That the infinite and finite cascade analysis predictions are in good agreement indicates that an experimental facility with a limited number of airfoils can potentially be used to model an infinite cascade provided that an effective means of dealing with the wind tunnel wall effects is found.

SUMMARY AND CONCLUSION

The unsteady aerodynamic influence coefficient technique has been investigated in a linear cascade for torsional airfoil oscillations at reduced frequencies up to 0.90 with 0.55 inlet Mach

number. Steady and unsteady airfoil surface pressure distributions were measured, the latter using flush-mounted miniature pressure transducers. Discrete Fourier analysis techniques were used to analyze the unsteady pressure data. Behavior of the unsteady pressure influence coefficients was examined in detail as were the convergence characteristics of the influence coefficient series. Predictions obtained from summation of the experimentally-determined influence coefficients were compared with experimental data obtained with all the airfoils oscillating simultaneously and the predictions of linearized unsteady aerodynamic analyses.

It was found that constraints introduced by the wind tunnel had detrimental effects on the data. First, the self-induced unsteady pressure distributions were found to vary with the location of the oscillating airfoil due to excitation of undesirable wind tunnel acoustic modes. Second, a relatively minor effect was found when the instrumented airfoil was located adjacent to the upper wind tunnel wall. In that case, reflection of pressure disturbances off the wall onto the adjacent airfoil surface caused small but undesirable effects. And third, relatively large unsteady pressures were found on the airfoils upstream of the oscillating airfoil. These were shown to result from excitation of an undesirable acoustic mode of the wind tunnel. This effect increased with increasing reduced frequency and caused the influence coefficient series for C_p to be nonconvergent at the largest reduced frequency. However, the ΔC_p series was convergent due to cancellation effects.

Undesirable effects aside, the predicted unsteady pressure difference coefficients obtained by the experimental influence coefficient technique are in good agreement with the available experimental data for all airfoils oscillating and the linearized analysis predictions. This agreement is an indication that the experimentally-determined values of ΔC_p are valid. But this is due, in part, to the cancellation that occurred when ΔC_p was calculated. Presumably, if the airfoils were highly loaded, differences between the lower and upper surface mean flow gradients might distort the waves to the extent that cancellation would be greatly reduced, and the plane wave mode of the wind tunnel would render even ΔC_p results invalid.

As it stands, the unsteady aerodynamic influence technique is of limited usefulness in this linear cascade. To reduce the effects of the wind tunnel walls, an effort is currently under way to replace the solid walls with porous walls designed to absorb incident acoustic waves using technology developed to reduce aircraft gas turbine engine noise (Groeneweg and Rice, 1987).

ACKNOWLEDGEMENTS

The experiments were performed with the technical assistance of R. Olsey, S. Orahoske and V. Verhoff. Helpful comments on the contents of this paper were provided by D. Huff and D. Hoyniak.

REFERENCES

Bölcs, A., Fransson, T.H. And Schläfli, D., 1989, "Aerodynamic Superposition Principle in Vibrating Turbine Cascades," AGARD-CPP-468/469, 1989.

Buffum, D.H. and Fleeter, S., 1990a, "Oscillating Cascade Aerodynamics by an Experimental Influence Coefficient Technique," Journal of Propulsion, Vol. 6, No. 5, Sept.-Oct. 1990, pp. 612-620.

Buffum, D.H. and Fleeter, S., 1990b, "Aerodynamics of a Linear Oscillating Cascade," NASA Technical Memorandum 103250.

Buffum, D.H. and Fleeter, S., 1993, "Wind Tunnel Wall Effects in a Linear Oscillating Cascade," Journal of Turbomachinery, Vol. 115, No.1, January 1993, pp. 147-156.

Davies, M.R.D. and Whitehead, D.S., 1984, "Unsteady Aerodynamic Measurements in a Transonic Annular Cascade," Unsteady Aerodynamics of Turbomachines and Propellers, Cambridge University Engineering Department, Cambridge, pp. 487-502.

Groeneweg, J.F. and Rice, E.J., 1987, "Aircraft Turbofan Noise," Journal of Turbomachinery, Vol. 109, pp. 130-141.

Hanamura, Y., Tanaka, H. and Yamaguchi, K., 1980, "A Simplified Method to Measure Unsteady Forces Acting on the Vibrating Blades in Cascade," Bulletin of the JSME, Vol. 23, No. 180, pp.880-887.

Kline, S.J. and McClintock, F.A., 1953, "Describing Uncertainties in Single-Sample Experiments," Mechanical Engineering, pp. 3-8.

Kobayashi, H., 1989, "Annular Cascade Study of Low Back-Pressure Supersonic Fan Blade Flutter," ASME paper 89-GT-297.

Mehmed, O., Kaza, K.R.V., Lubomski, J.F. and Kielb, R.E., 1982, "Bending-Torsion Flutter of a Highly Swept Advanced Turboprop," NASA Technical Memorandum 82975.

Richards, E.J. and Mead, D.J., editors, 1968, Noise and Acoustic Fatigue in Aeronautics, John Wiley & Sons, London.

Széchényi, E., 1985, "Fan Blade Flutter - Single Blade Instability or Blade to Blade Coupling?," ASME Paper 85-GT-216.

Smith, S.N., 1972, "Discrete Frequency Sound Generation in Axial Flow Turbomachines," Aeronautical Research Council Reports and Memoranda No. 3709.

Whitehead, D.S., 1987, "Classical Two-Dimensional Methods," AGARD Manual on Aeroelasticity in Axial Flow Turbomachines, Volume 1: Unsteady Turbomachinery Aerodynamics, AGARDograph No. 298, pp. 3-1 - 3-30.

Appendix

Cutoff conditions for acoustic waves in rectangular ducts with a uniform mean flow will be found. The book by Richards and Mead (1968) derived such conditions, however, the cutoff condition they obtained for downstream-running waves is too restrictive, as will now be shown. Most of the following derivation follows their approach exactly - the error they made was in the interpretation of their solution.

A uniform, inviscid mean flow of speed V is assumed to exist along the z-axis of an infinite rectangular duct of width A and height B. Solutions to the convective wave equation

$$\nabla^2 p - \frac{1}{a^2}\frac{D^2 p}{Dt^2} = 0 \tag{1}$$

are sought for the perturbation pressure p. a is the mean speed of sound and D/Dt is the time rate of change for an observer moving with the mean flow, $D/Dt = \partial/\partial t + V\partial/\partial z$. Harmonic pressure perturbations of the form $p(x,y,z)e^{i\omega t}$ are chosen to have the form

$$p(x,y,z)e^{i\omega t} = \cos(k_x x)\cos(k_y y)Z(z)e^{i\omega t} \tag{2}$$

in order to satisfy the zero normal velocity condition at the duct walls located at x=0,A and y=0,B. k_x and k_y are the x and y components of the wavenumber:

$$k_x = l\pi/A, \quad l = 0, 1, 2, \ldots$$

and

$$k_y = m\pi/B, \quad m = 0, 1, 2, \ldots$$

Substituting Equation 2 into Equation 1 and differentiating yields

$$\left[(1-M^2)\frac{d^2}{dz^2} - 2i\frac{\omega M}{a}\frac{d}{dz} + ((\frac{\omega}{a})^2 - K^2)\right]Z(z) = 0 \tag{3}$$

where M is the mean flow Mach number and $K^2 = k_x^2 + k_y^2$. Assuming

$$Z(z) = C_z e^{ik_z z}, \tag{4}$$

Equation 3 will be satisfied if

$$k_z = k_z^{\pm} = \frac{\omega M/a \pm \sqrt{(\omega/a)^2 - (1-M^2)K^2}}{1-M^2}. \tag{5}$$

The character of the solutions for k_z changes when the parameter values are such that $(\omega/a)^2 = (1-M^2)K^2$. When $(\omega/a)^2 < (1-M^2)K^2$, k_z is complex-valued. Splitting k_z into real (k_z^R) and imaginary (k_z^I) parts, Equation 4 becomes

$$Z(z) = C_z e^{i\left(k_z^R \pm ik_z^I\right)z} = C_z e^{ik_z^R z} e^{\pm k_z^I z}, \tag{6}$$

indicating that the waves either grow or decay exponentially with axial distance. The amplifying wave solution is commonly disallowed on the basis that it is not physically acceptable, leaving the decaying wave solution.

To have waves which propagate without attenuation, k_z must be real. Thus the condition

$$\left(\frac{\omega}{a}\right)^2 \geq (1-M^2)K^2 \tag{7}$$

must be met for propagating waves to exist.

The direction in which the propagating waves travel is determined by the group velocity, the velocity at which an observer tracking a particular disturbance travels. With respect to the mean flow, an acoustic disturbance travels at the speed of sound a in the direction opposite of the wave vector. Hence the disturbance velocity with respect to a fixed coordinate system, the group velocity, is the sum of the acoustic velocity and the mean flow velocity, i.e.,

$$\vec{V}_g = -a\frac{\vec{k}}{\left|\vec{k}\right|} + V\vec{e}_z. \tag{8}$$

$\vec{e}_z$ is a unit vector pointing along the duct axis and $\vec{k} = k_x\vec{e}_x + k_y\vec{e}_y + k_z\vec{e}_z$ is the wave vector. The group velocity in the z direction is therefore

$$V_{gz} = -a\frac{k_z}{\sqrt{k_z^2 + K^2}} + V \tag{9}$$

When $(\omega/a)^2 = (1-M^2)K^2$ (the 'acoustic resonance' condition),

$$K^2 = \frac{(\omega/a)^2}{1-M^2}, \tag{10}$$

and Equation 5 reduces to

$$k_z = \frac{\omega M}{a(1-M^2)}. \tag{11}$$

Using Equations 10 and 11, one obtains

$$\frac{k_z}{\sqrt{k_z^2 + K^2}} = M. \tag{12}$$

Substituting Equation 12 into Equation 9 results in $V_{gz} = -Ma + V = 0$. Thus, at the resonance condition, disturbances do not propagate along the duct. It is then clear that, when $(\omega/a)^2 > (1-M^2)K^2$ and $k_z = k_z^-$, $V_{gz} > 0$ and waves therefore will propagate downstream. Similarly, waves will propagate upstream ($V_{gz} < 0$) when $(\omega/a)^2 > (1-M^2)K^2$ and $k_z = k_z^+$. Therefore the appropriate condition for waves propagating both upstream and downstream is

$$\left(\frac{\omega}{a}\right)^2 > (1-M^2)K^2. \tag{13}$$

Richards and Mead obtained the correct result for the upstream-traveling waves but have $(\omega/a)^2 > K^2$ as the condition for waves traveling downstream without attenuation. They erred in requiring that the z-component of the phase velocity, $-\omega/k_z$, be positive rather than requiring that the z-component of the group velocity be positive. Even though the phase velocity will be negative when $(1-M^2)K^2 < (\omega/a)^2 < K^2$, the group velocity is positive due to convection by the mean flow.

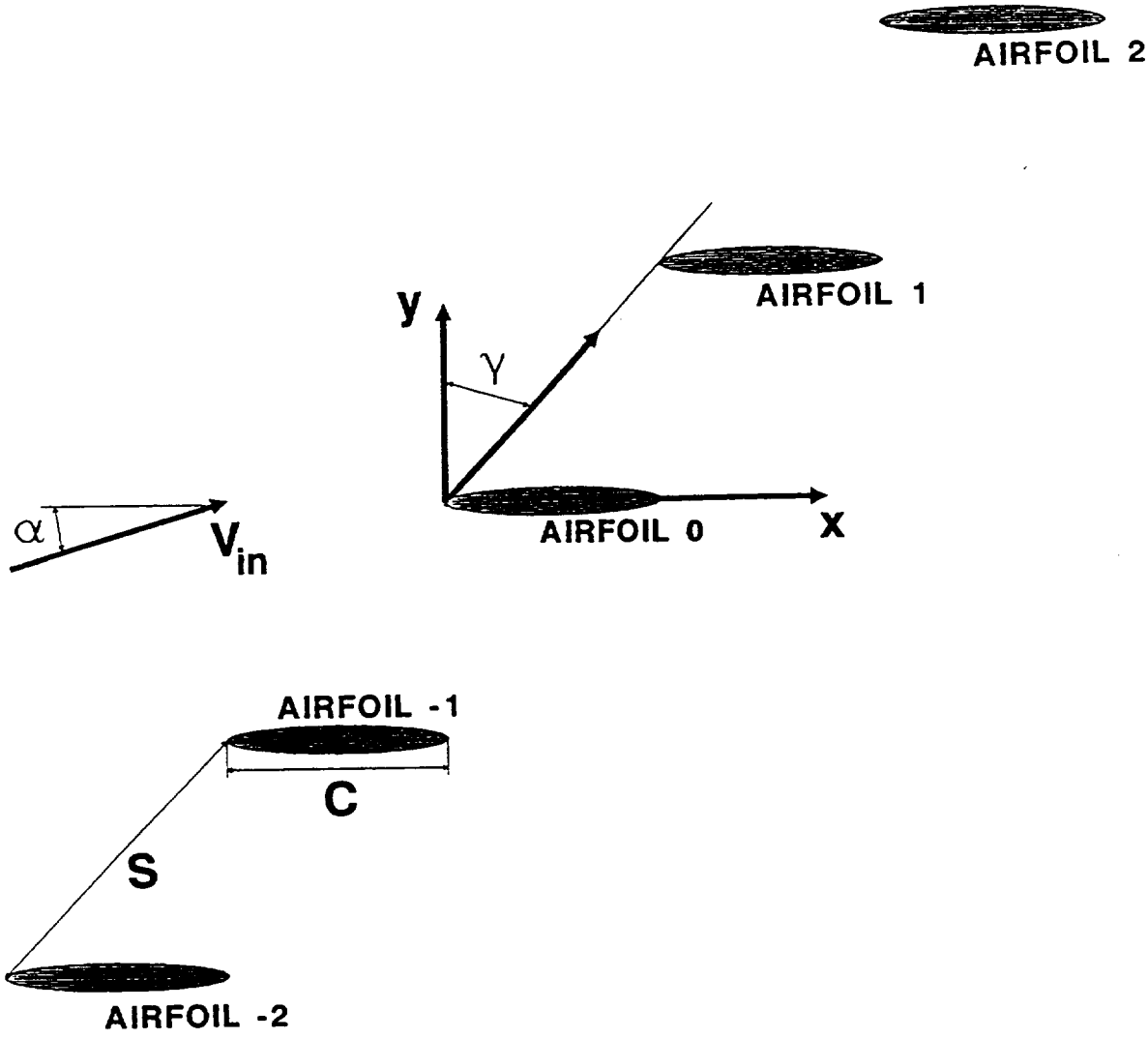

Figure 1 Cascade geometry

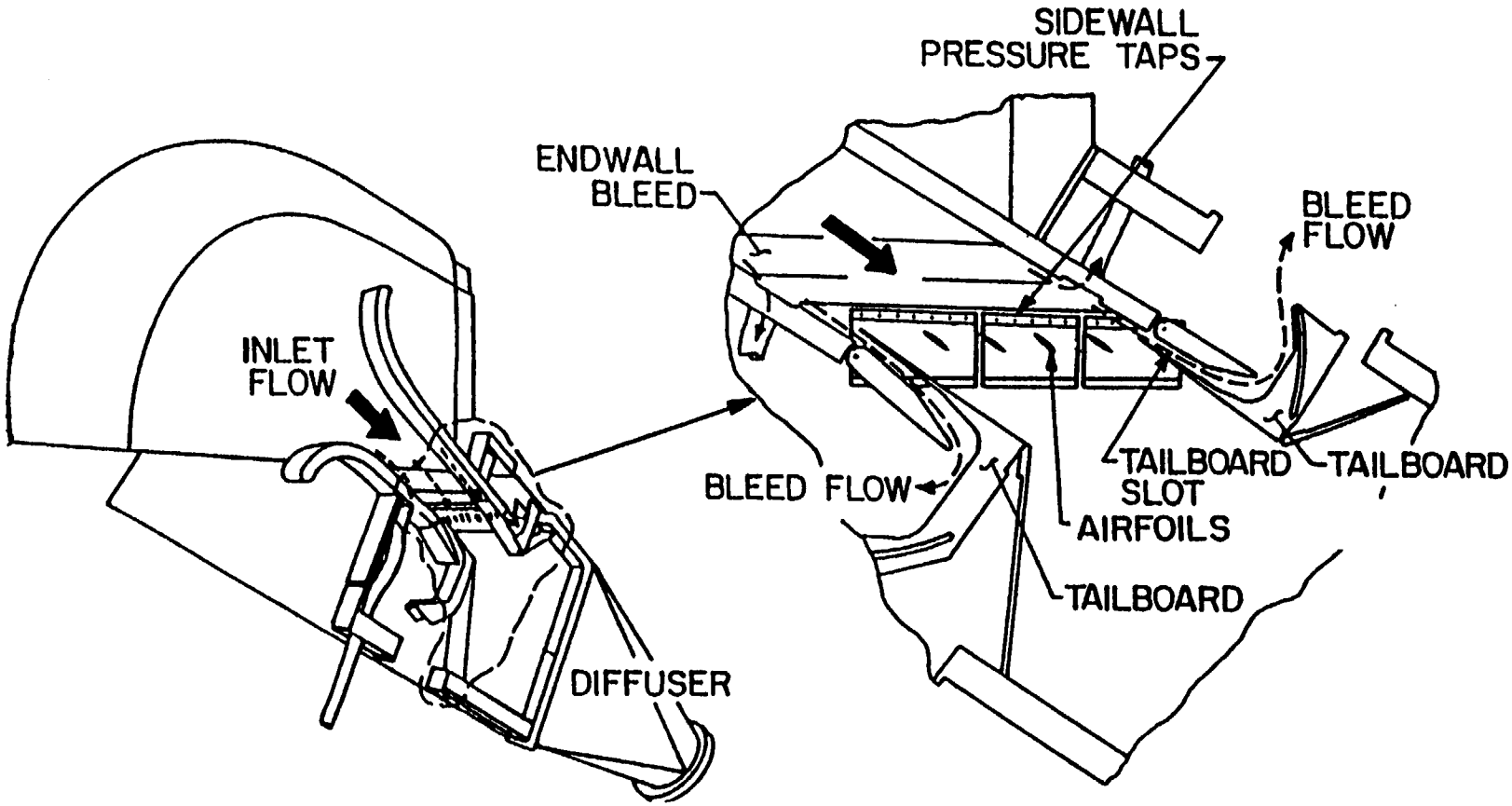

Figure 2 Oscillating cascade facility

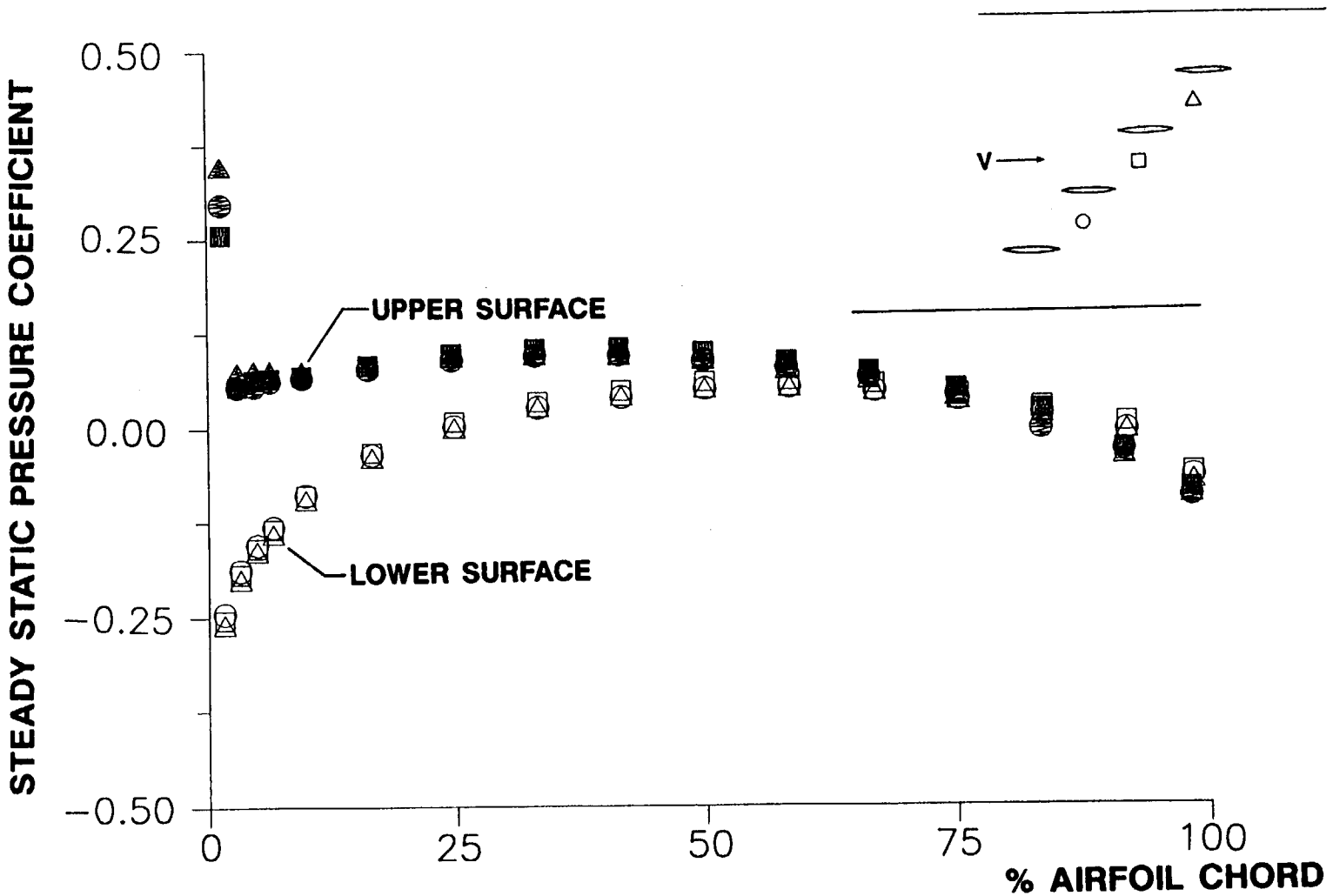

Figure 3 Airfoil surface steady pressure coefficient distributions, M = 0.55, α_0 = 2 degrees

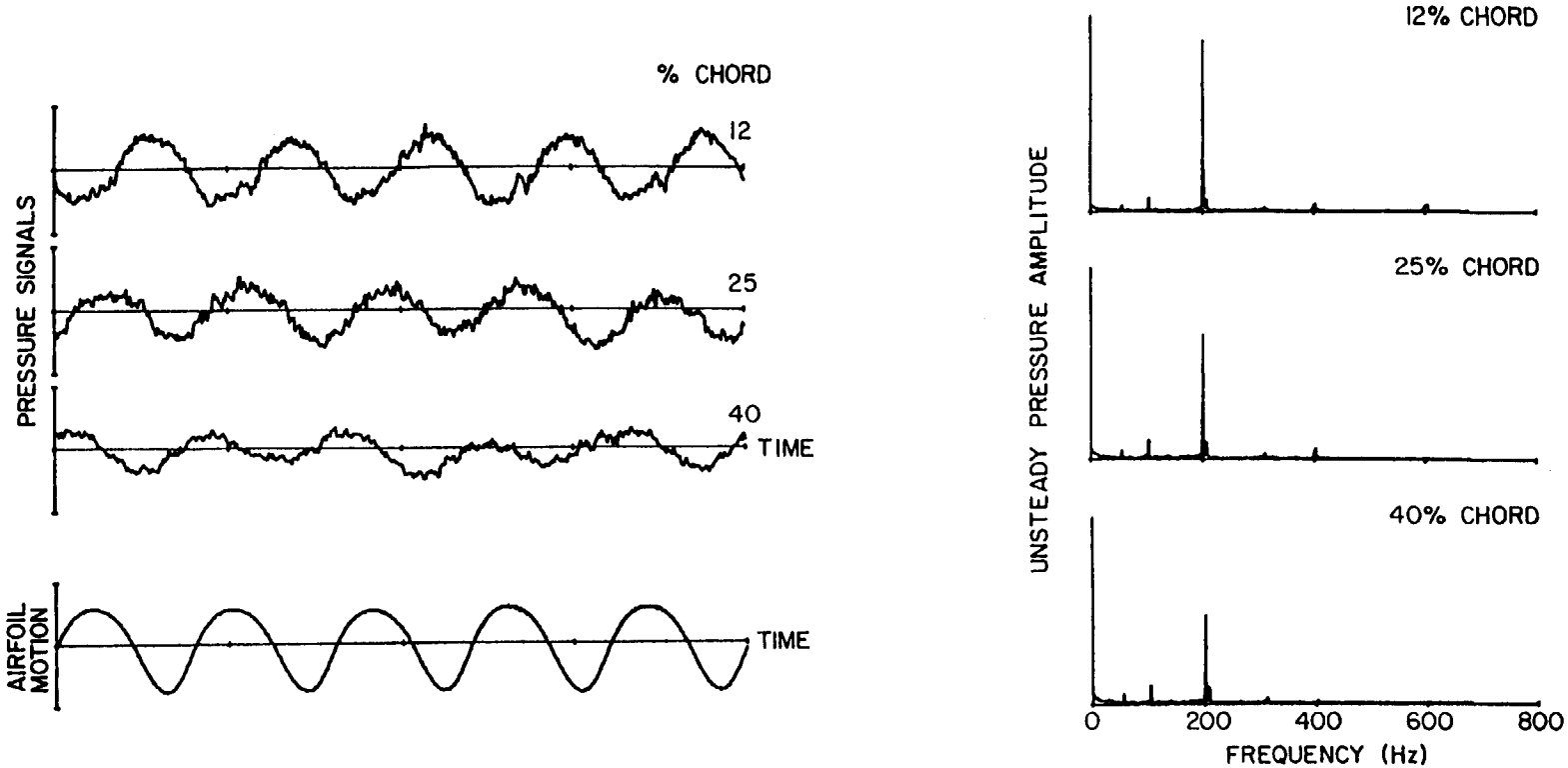

Figure 4 Time-dependent signals and averaged pressure spectra

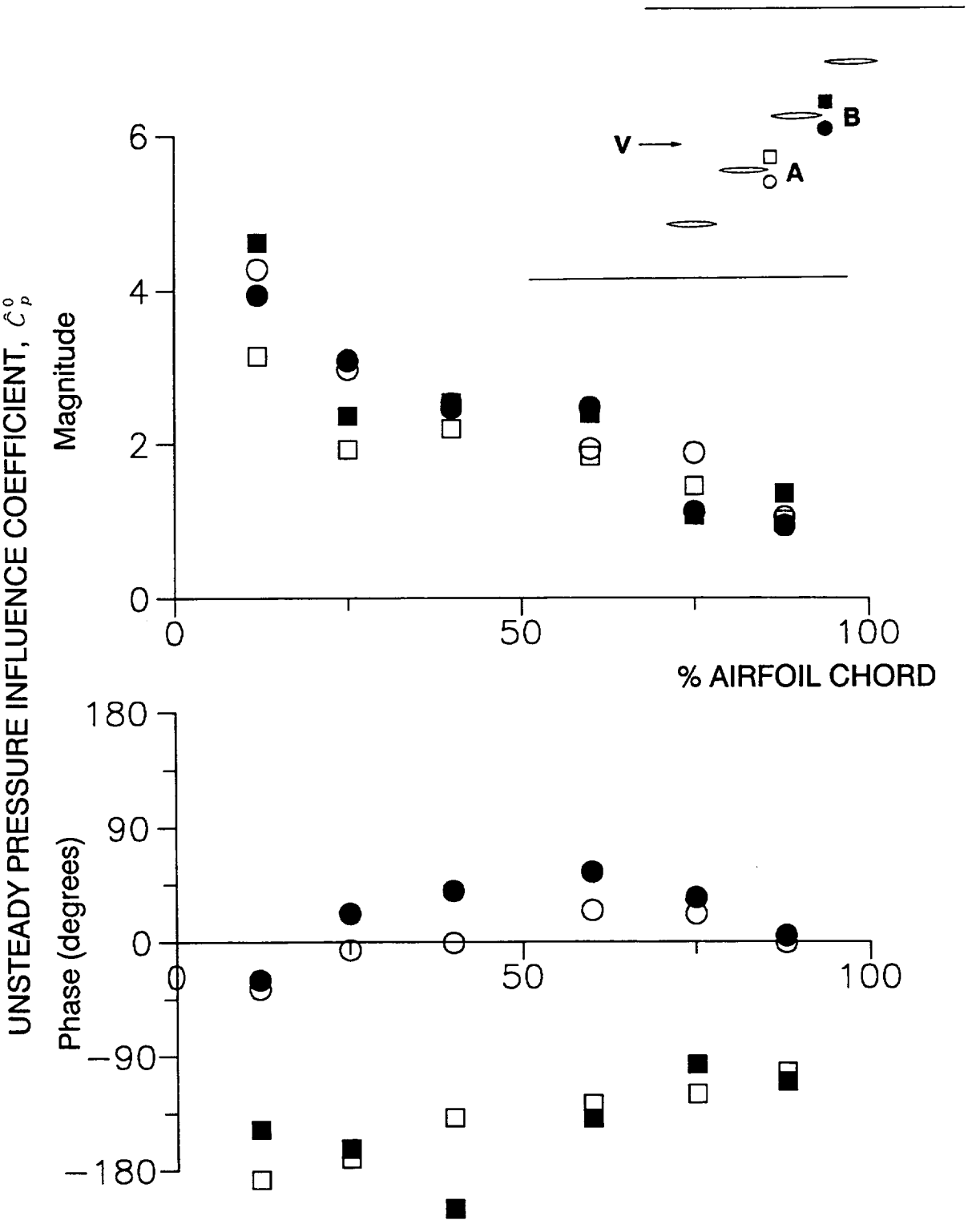

Figure 5 Cascade dynamic periodicity, oscillating airfoil in relative position 0, k = 0.90

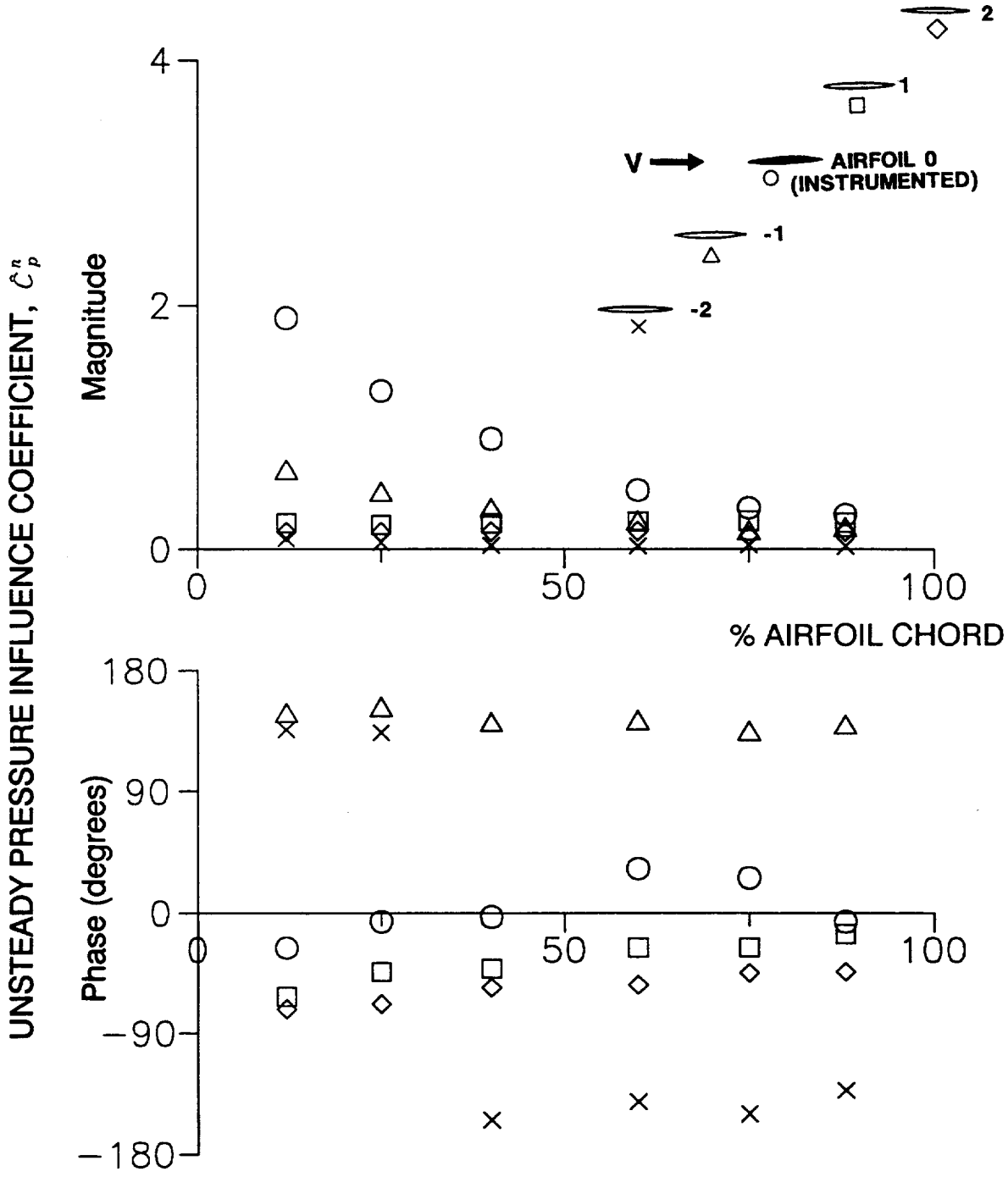

Figure 6 Airfoil lower surface unsteady pressure influence coefficient distribution as a function of the oscillating airfoil relative position, k = 0.40

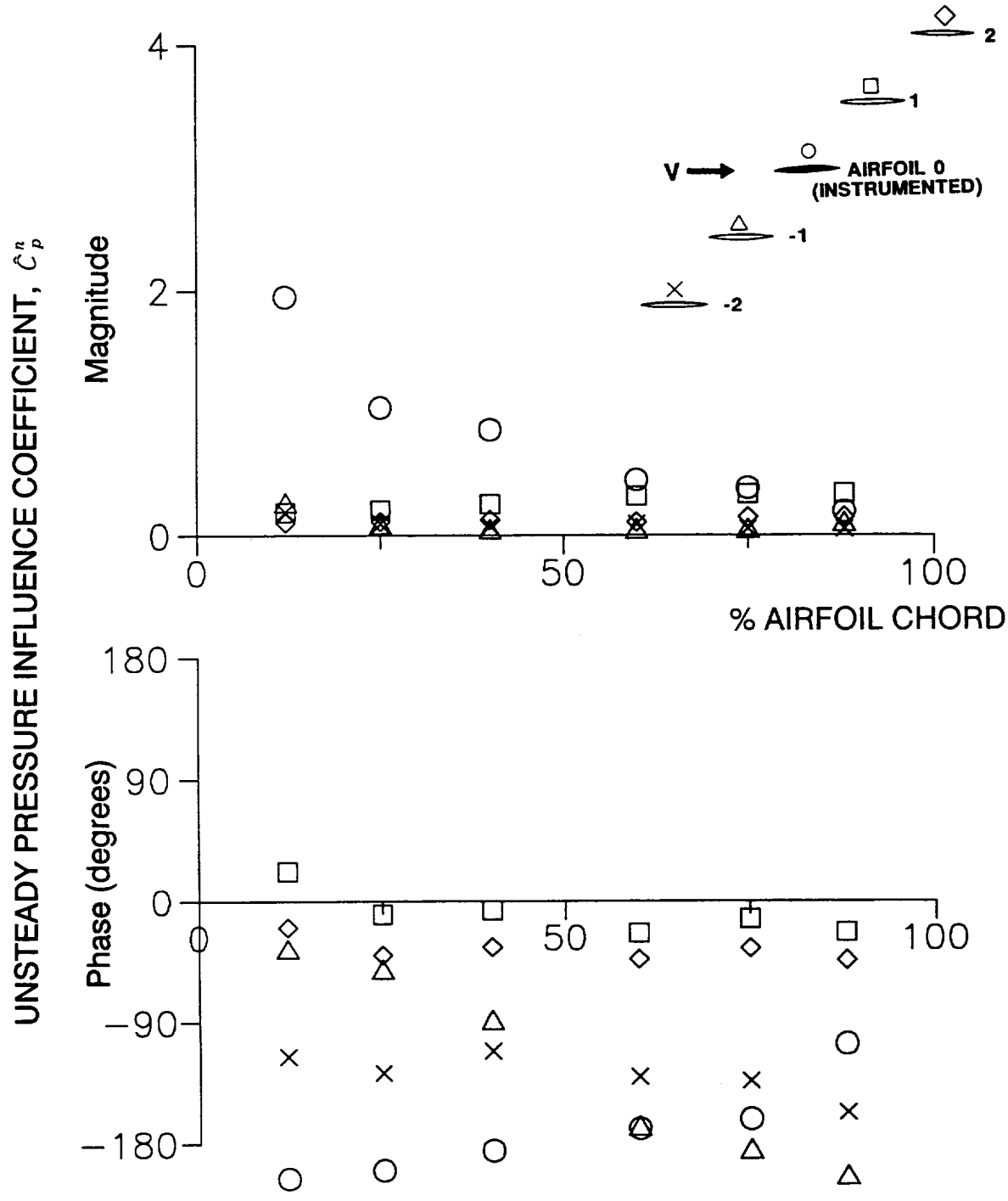

Figure 7 Airfoil upper surface unsteady pressure influence coefficient distribution as a function of the oscillating airfoil relative position, k = 0.40

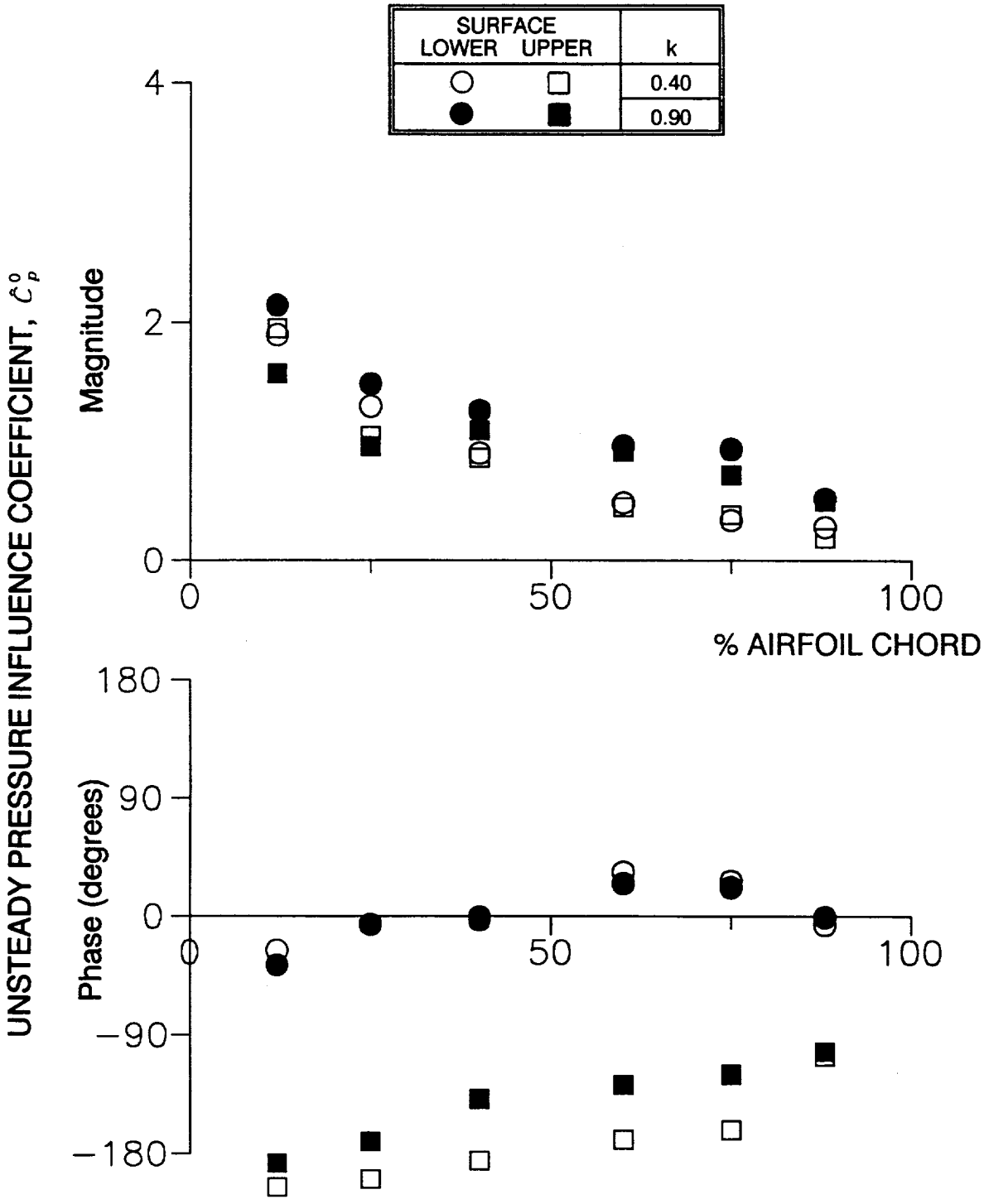

Figure 8 Effect of reduced frequency on unsteady pressure influence coefficient, oscillating airfoil in relative position 0

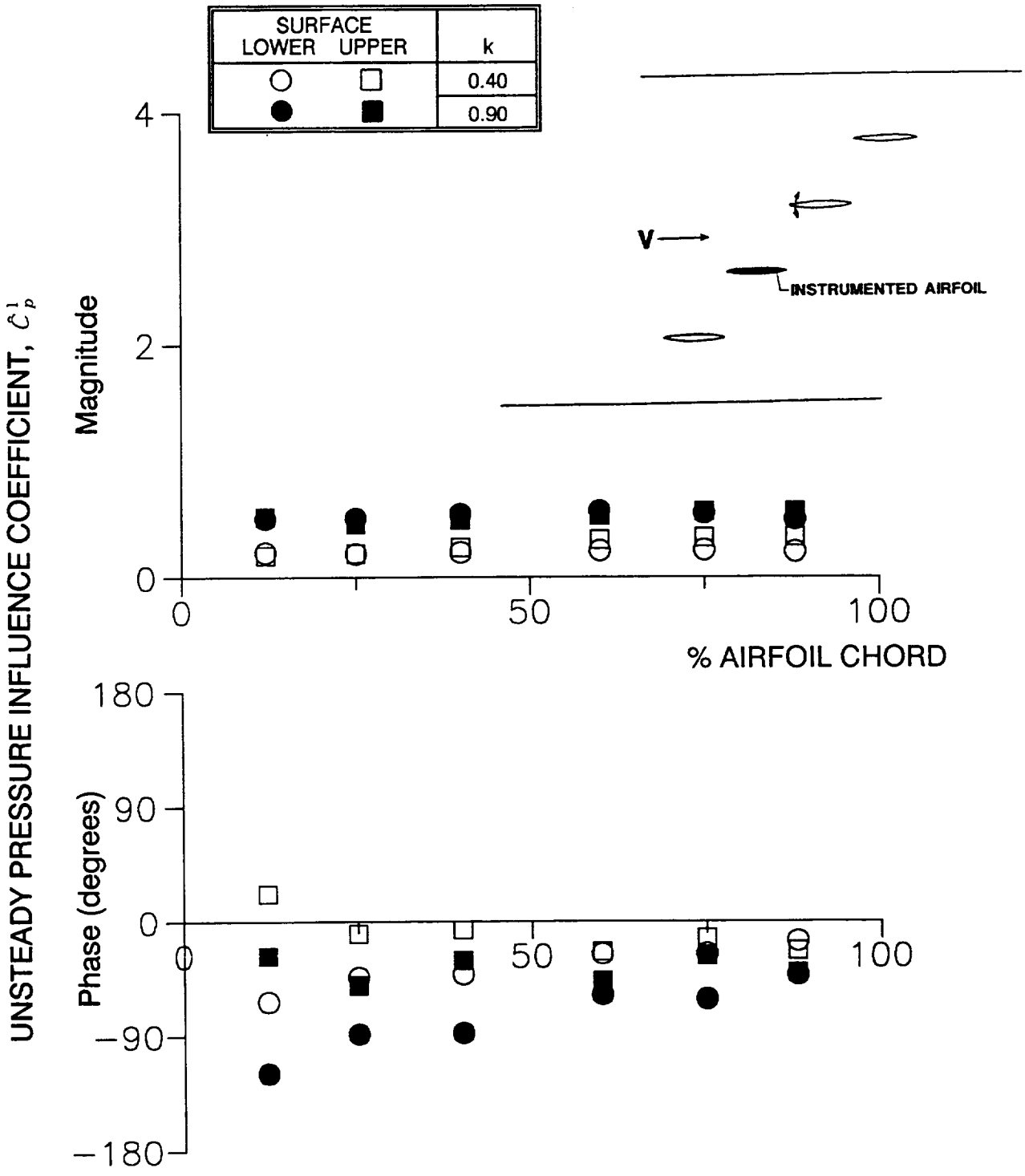

Figure 9 Effect of reduced frequency on unsteady pressure influence coefficient, oscillating airfoil in relative position 1

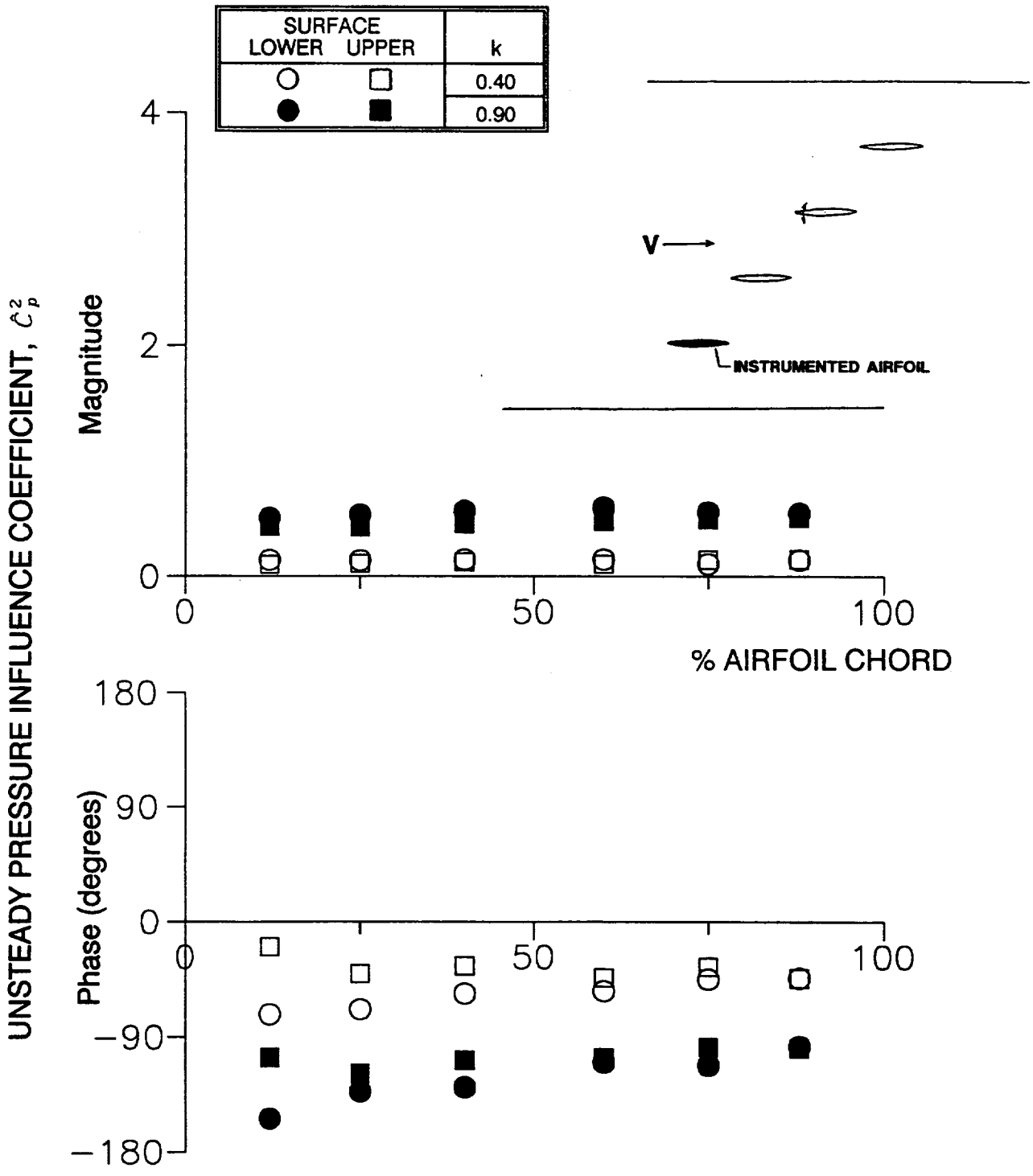

Figure 10 Effect of reduced frequency on unsteady pressure influence coefficient, oscillating airfoil in relative position 2

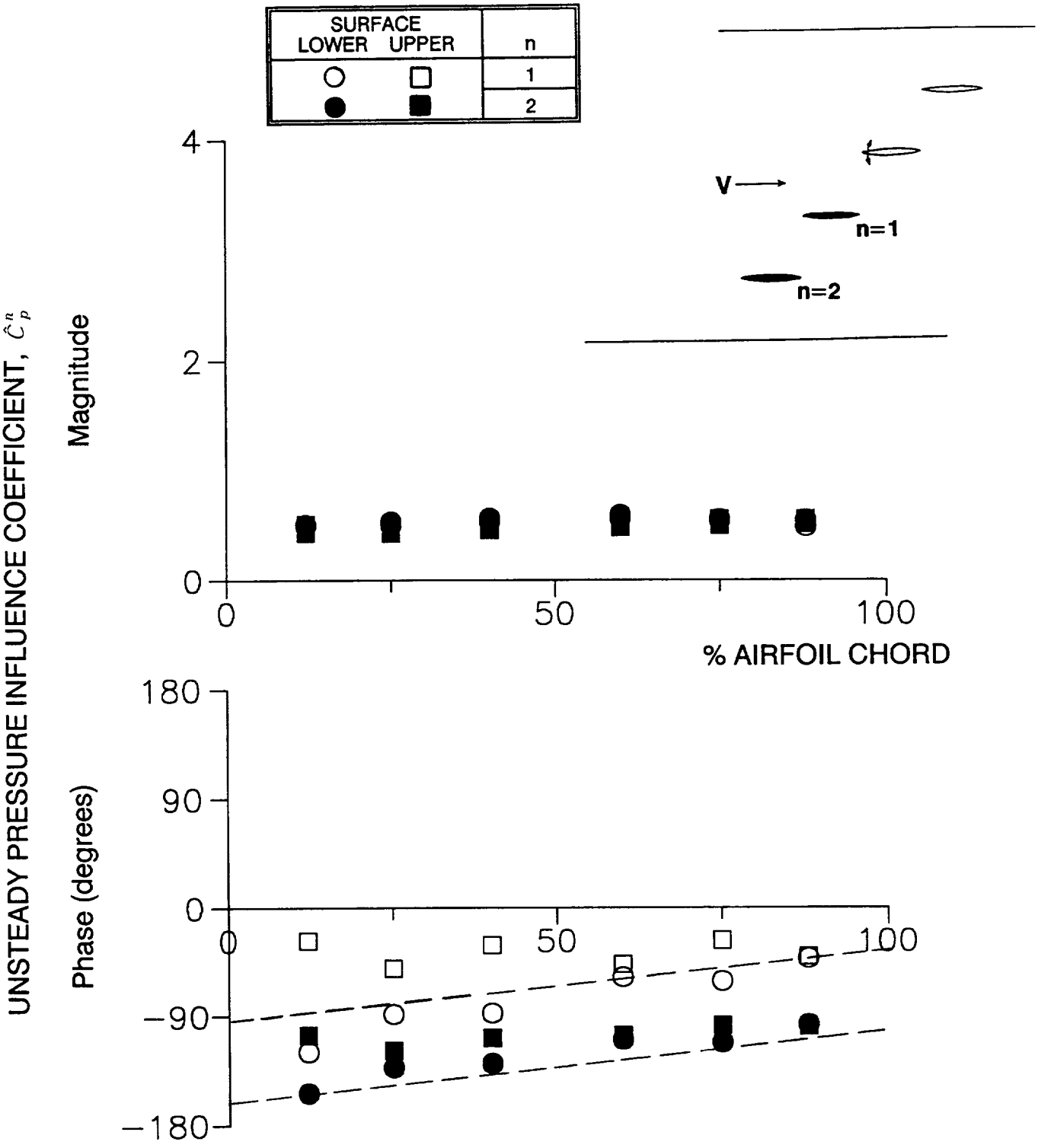

Figure 11 Effect of oscillating airfoil relative position on unsteady pressure influence coefficient, k=0.90

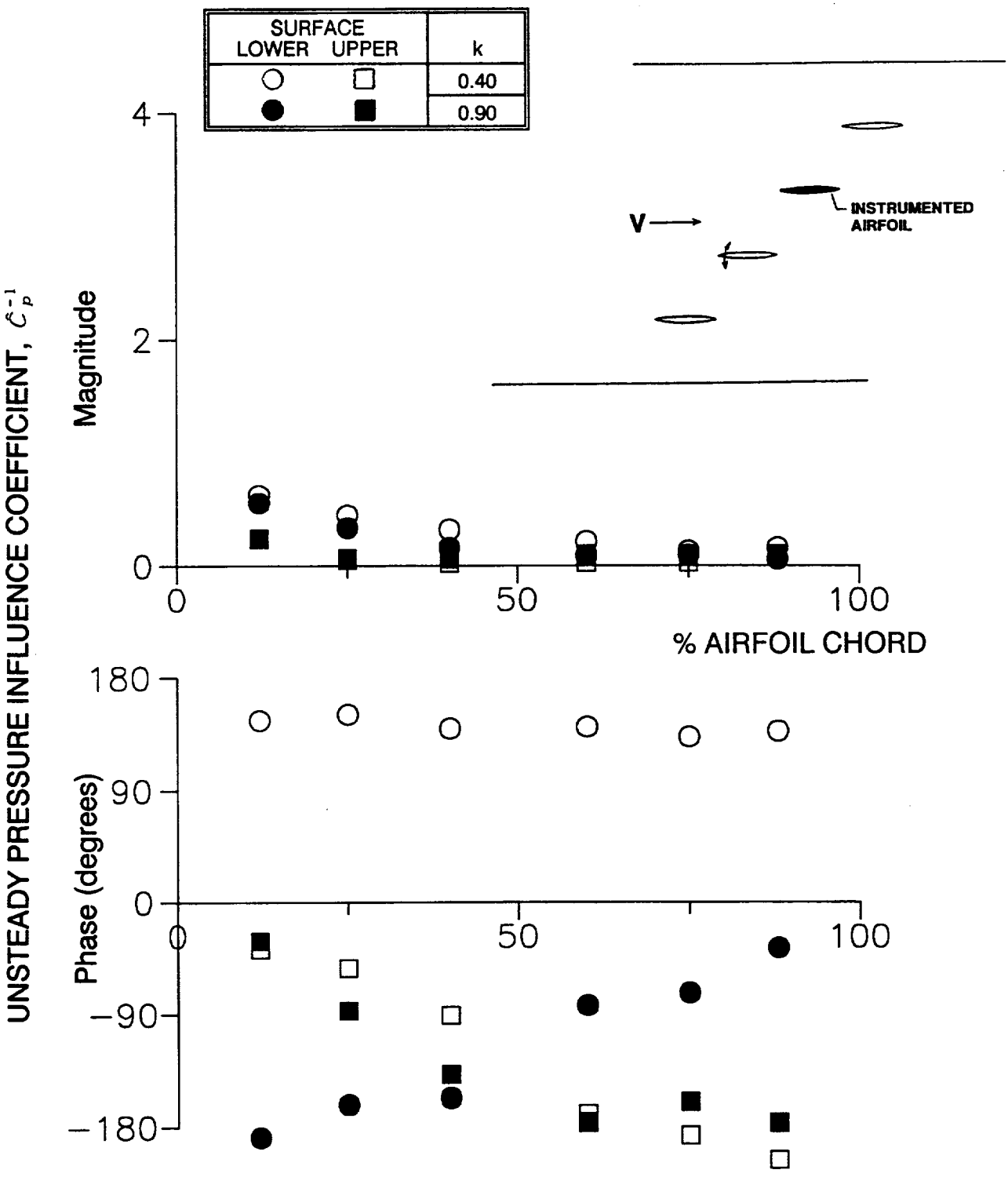

Figure 12 Effect of reduced frequency on unsteady pressure influence coefficient, oscillating airfoil in relative position -1

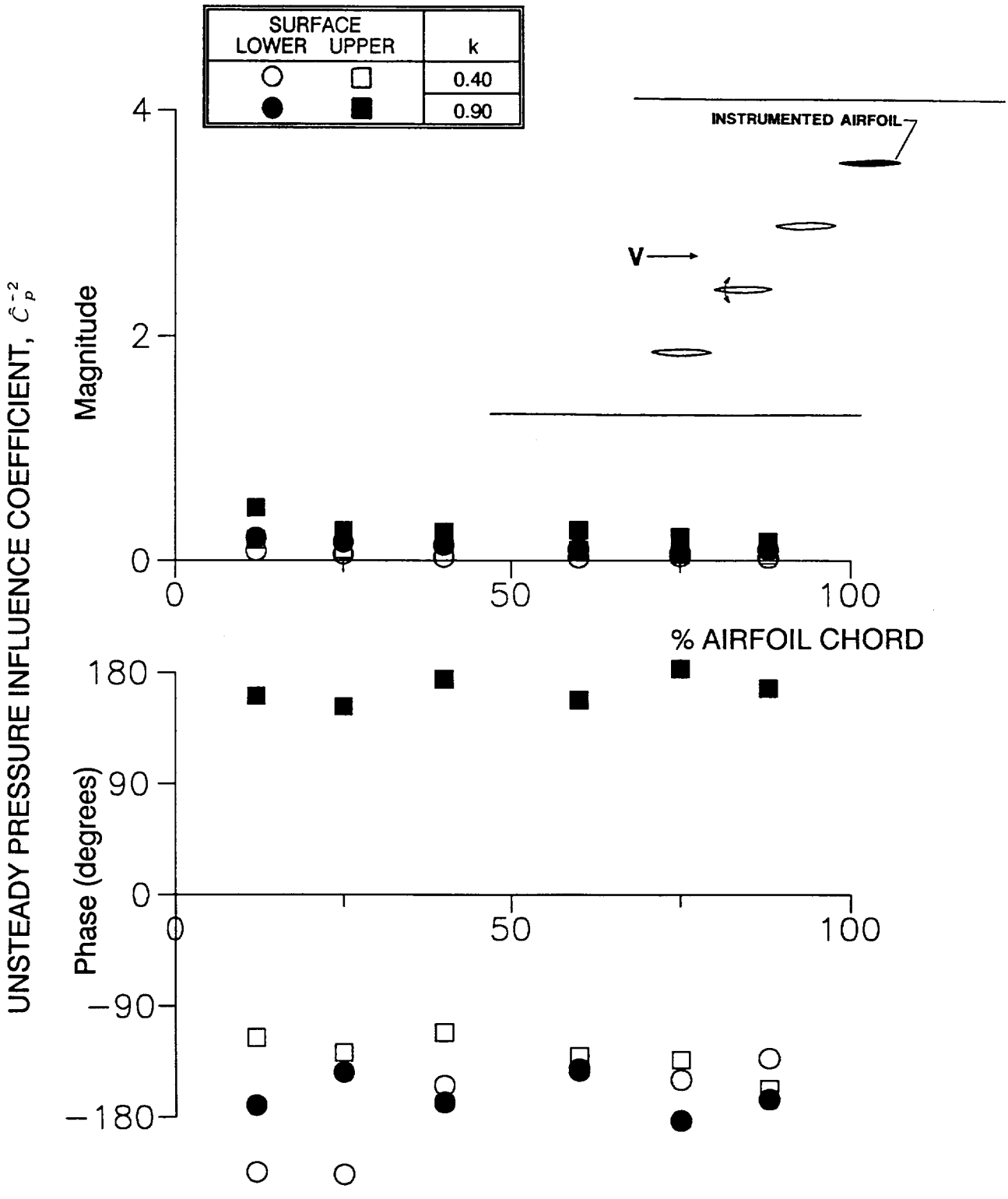

Figure 13 Effect of reduced frequency on unsteady pressure influence coefficient, oscillating airfoil in relative position -2

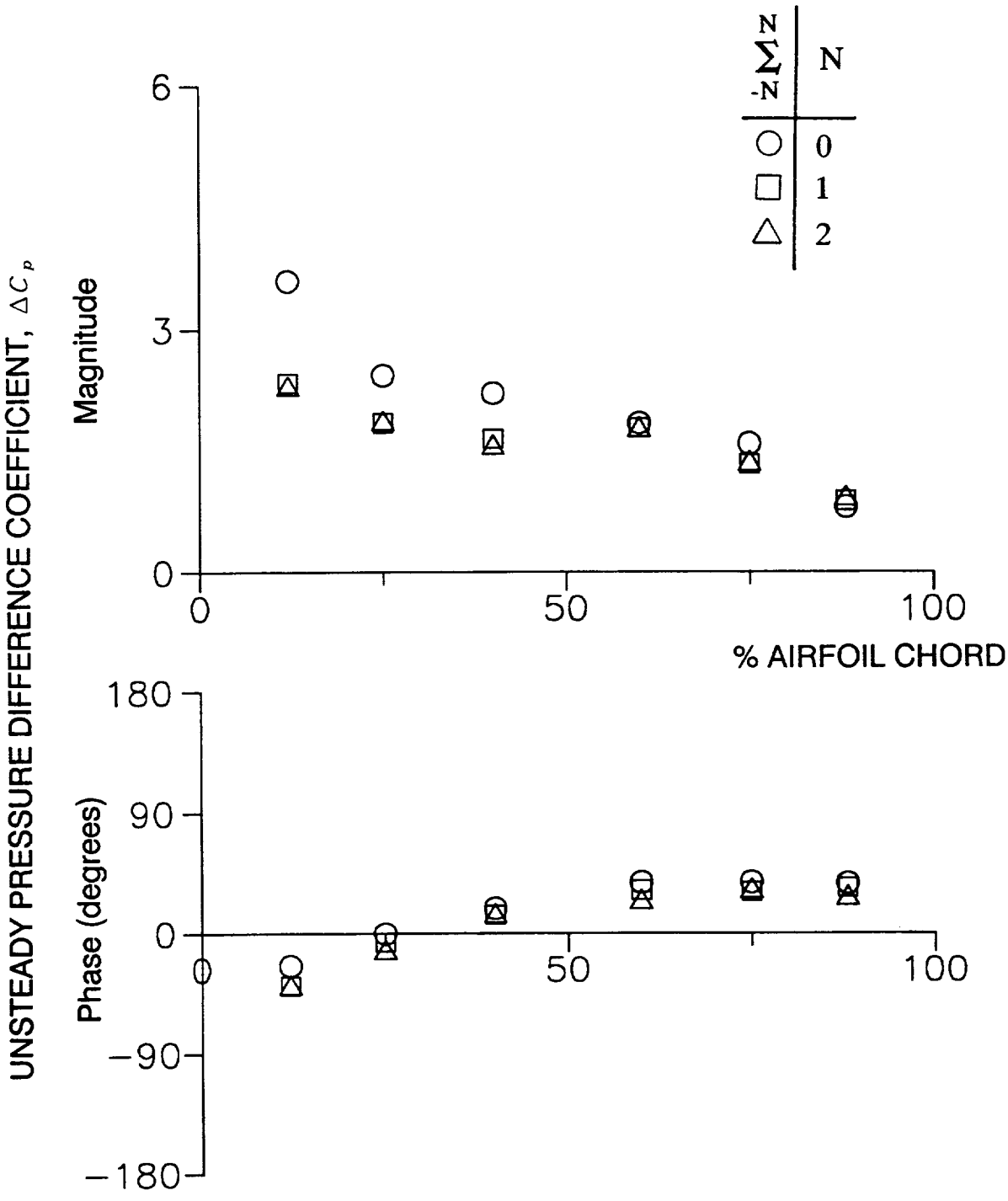

Figure 14 Summation of unsteady pressure difference influence coefficients, k = 0.90, β = 0 degrees

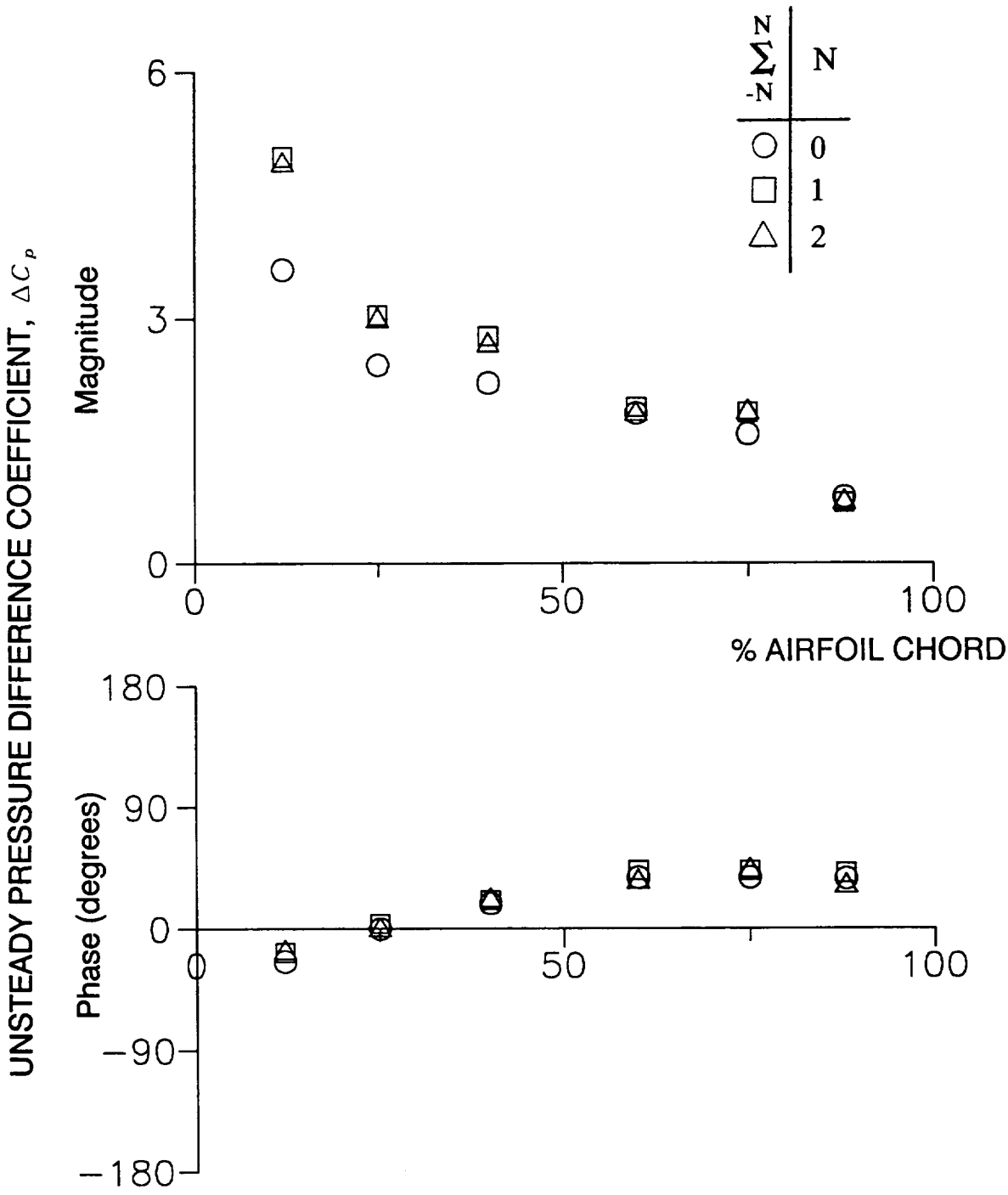

Figure 15 Summation of unsteady pressure difference influence coefficients, k=0.90, β =180 degrees

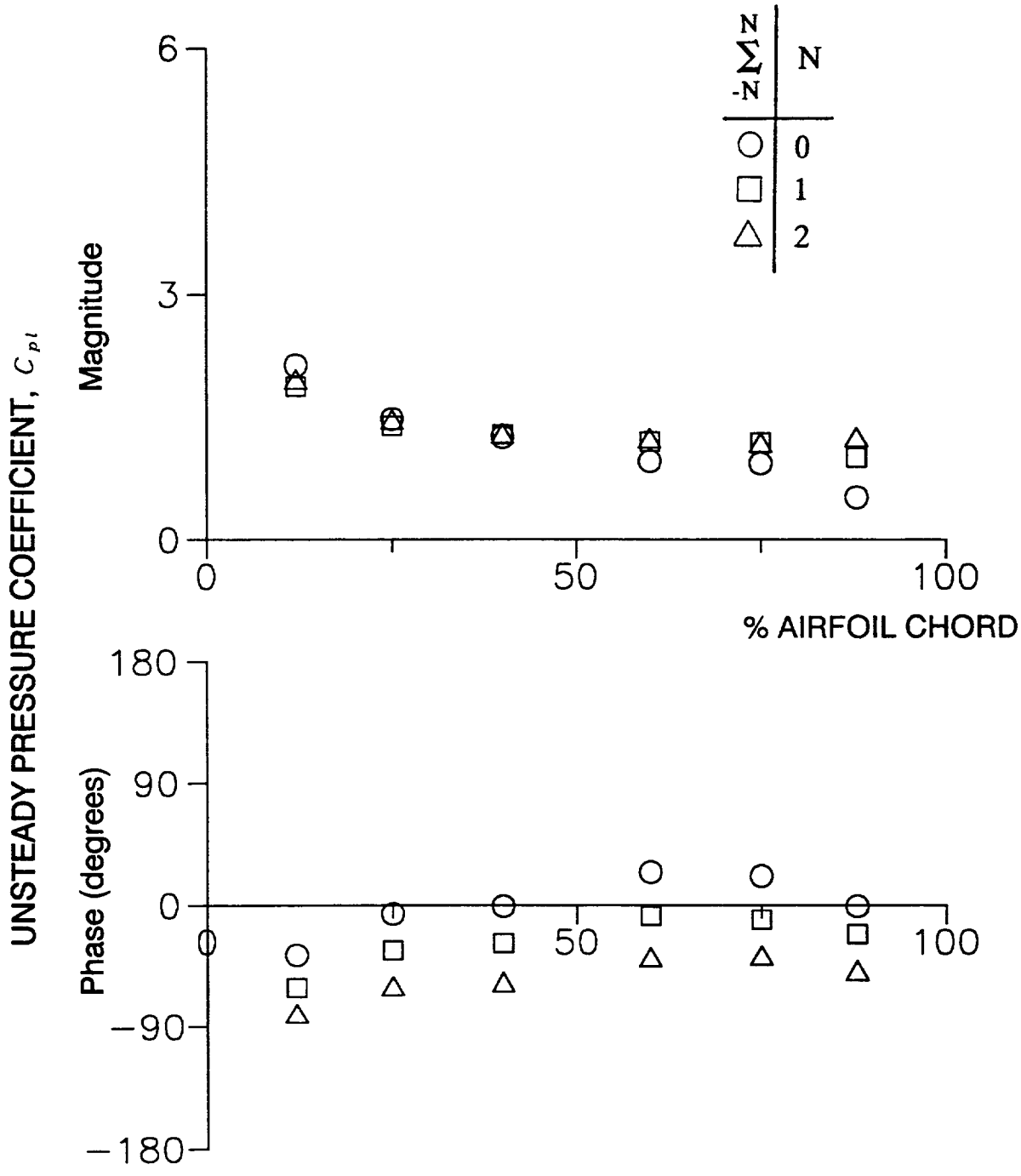

Figure 16 Summation of airfoil lower surface unsteady pressure influence coefficients, k = 0.90, β = 0 degrees

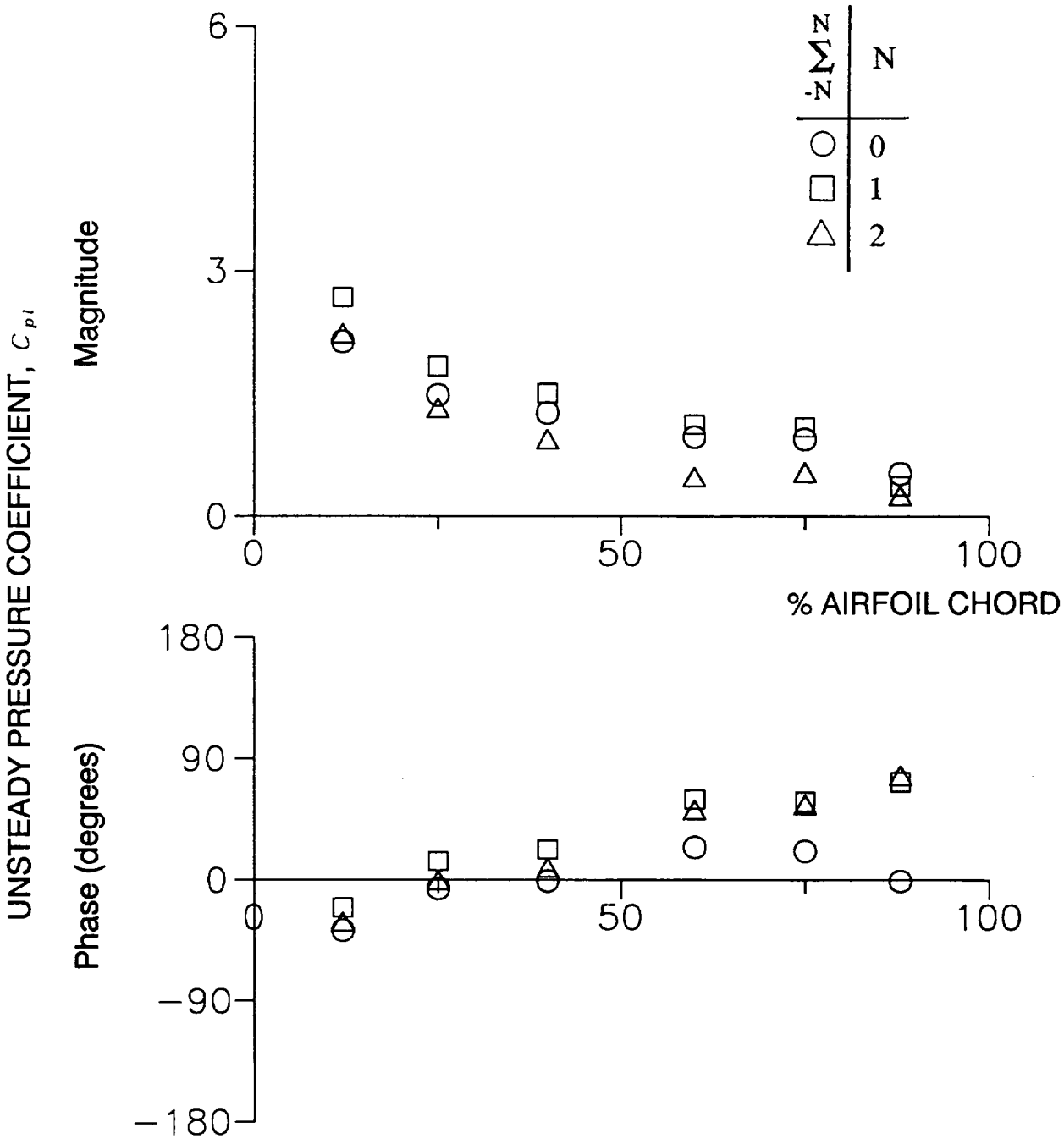

Figure 17 Summation of airfoil lower surface unsteady pressure influence coefficients, k=0.90, β =180 degrees

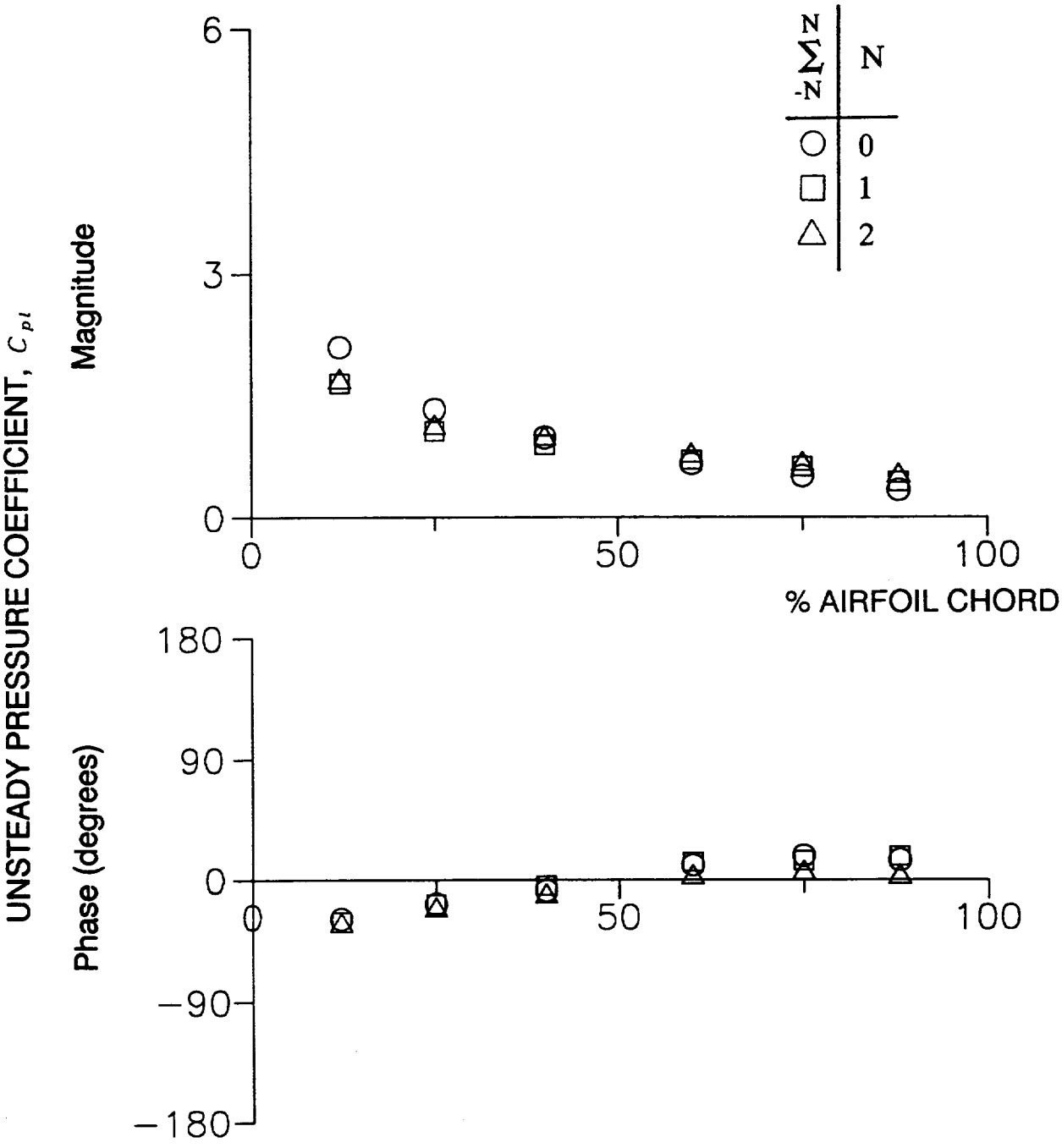

Figure 18 Summation of airfoil lower surface unsteady pressure influence coefficients, k=0.40, β =0 degrees

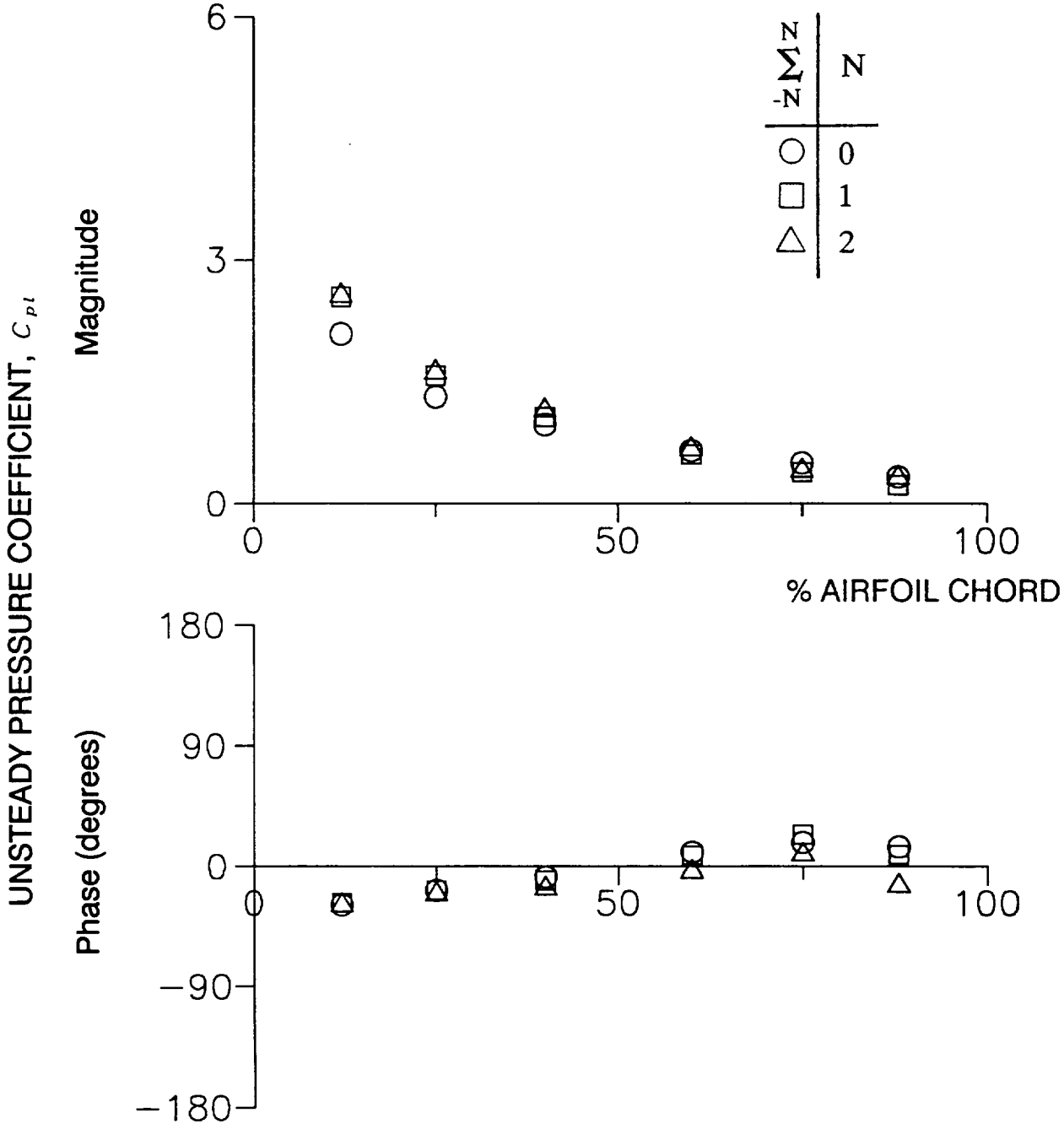

Figure 19 Summation of airfoil lower surface unsteady pressure influence coefficients, k=0.40, β=180 degrees

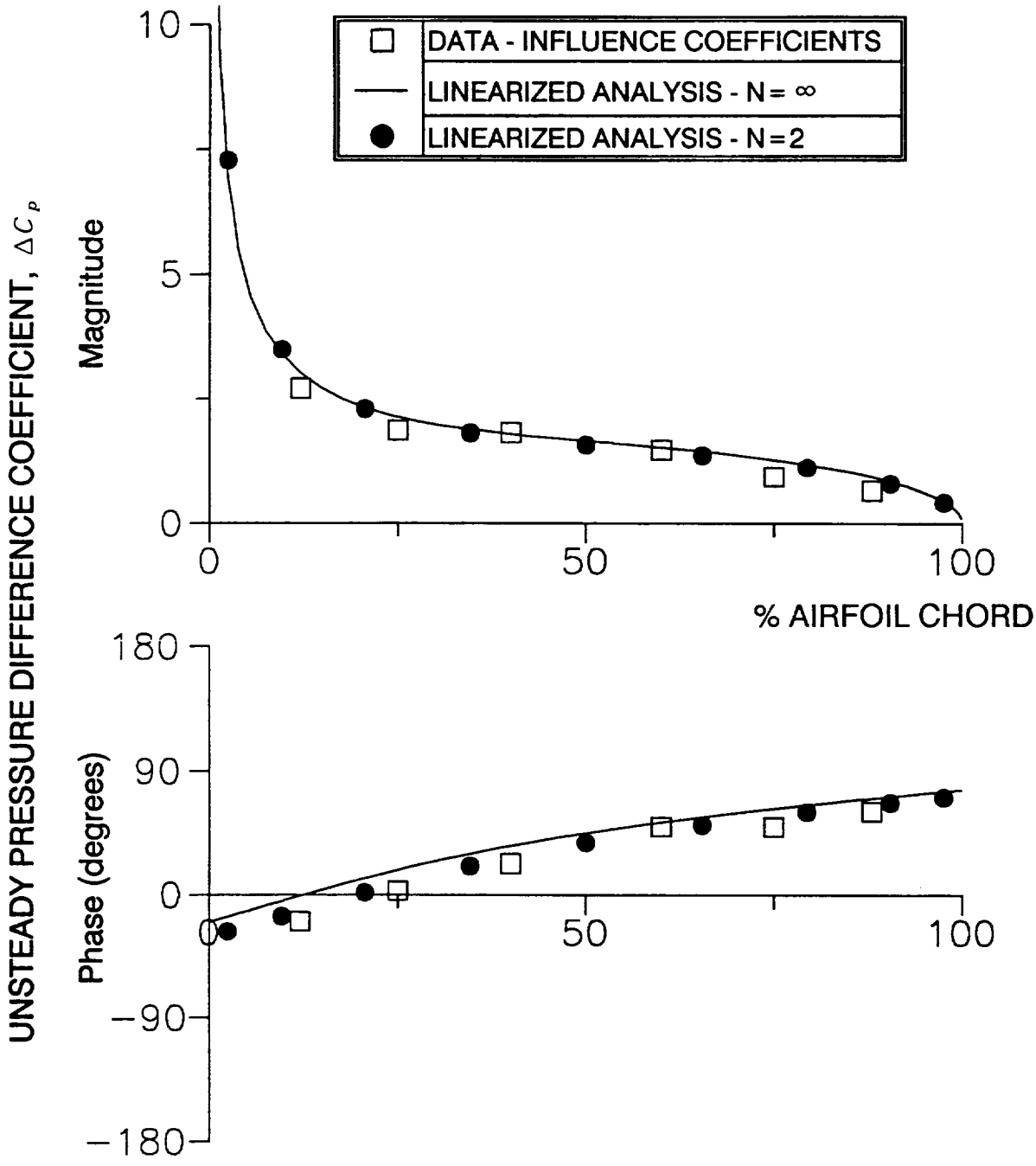

Figure 20 Unsteady pressure difference coefficient distribution, k = 0.64, $\beta = 0$

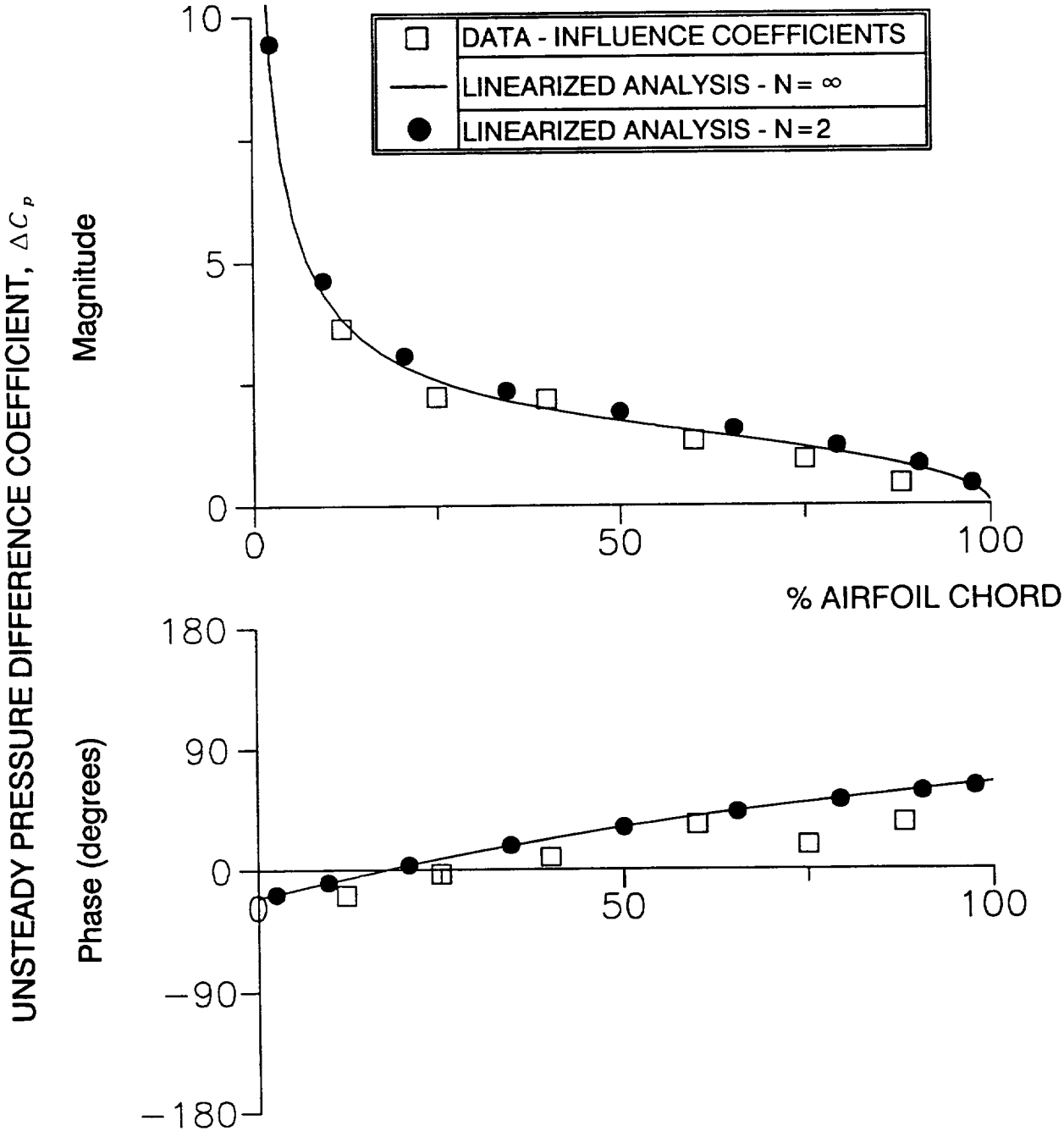

Figure 21 Unsteady pressure difference coefficient distribution, k = 0.64, $\beta = 45$

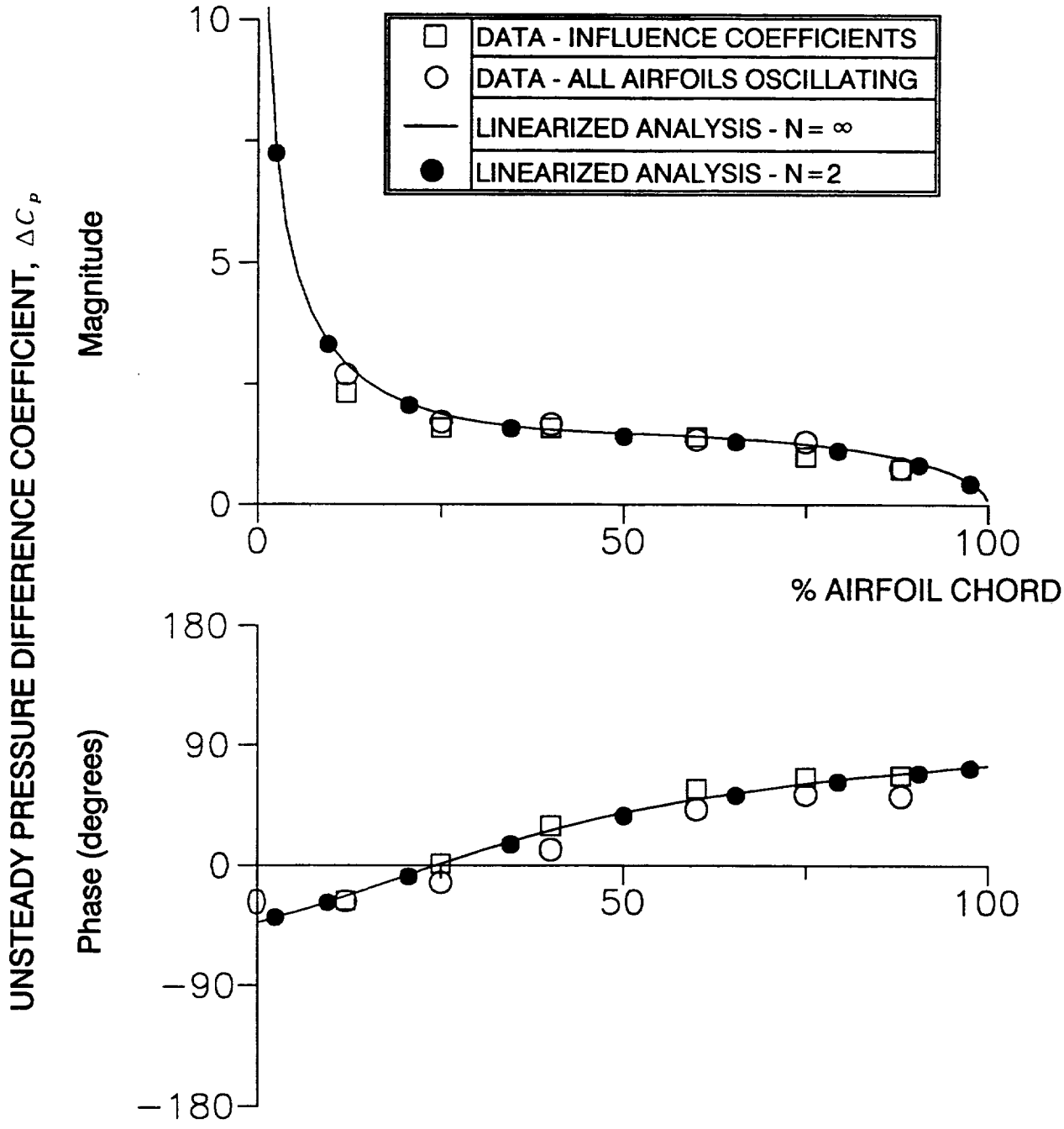

Figure 22 Unsteady pressure difference coefficient distribution, k = 0.64, β = -45 degrees

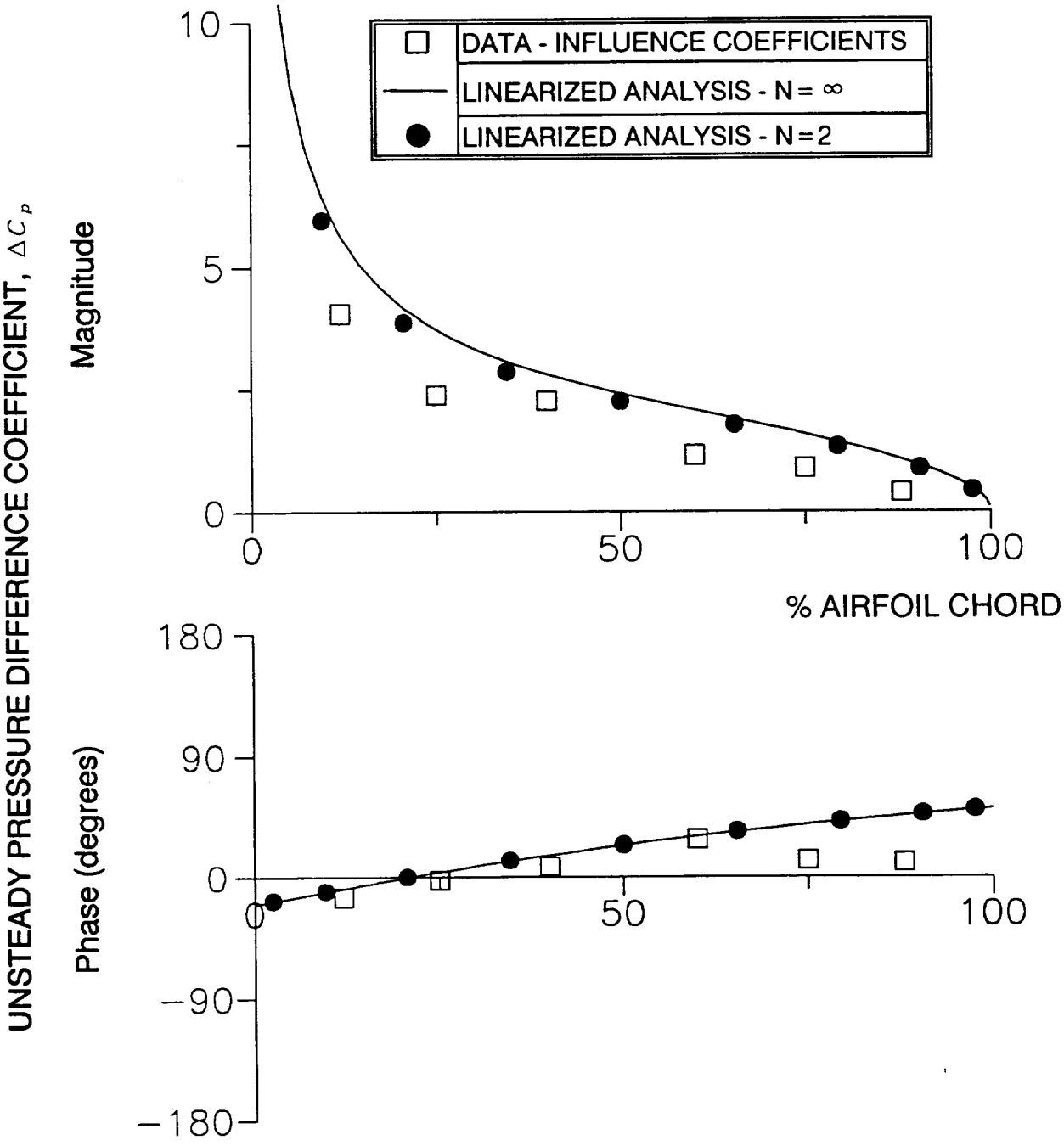

Figure 23 Unsteady pressure difference coefficient distribution, k = 0.64, β = 90 degrees

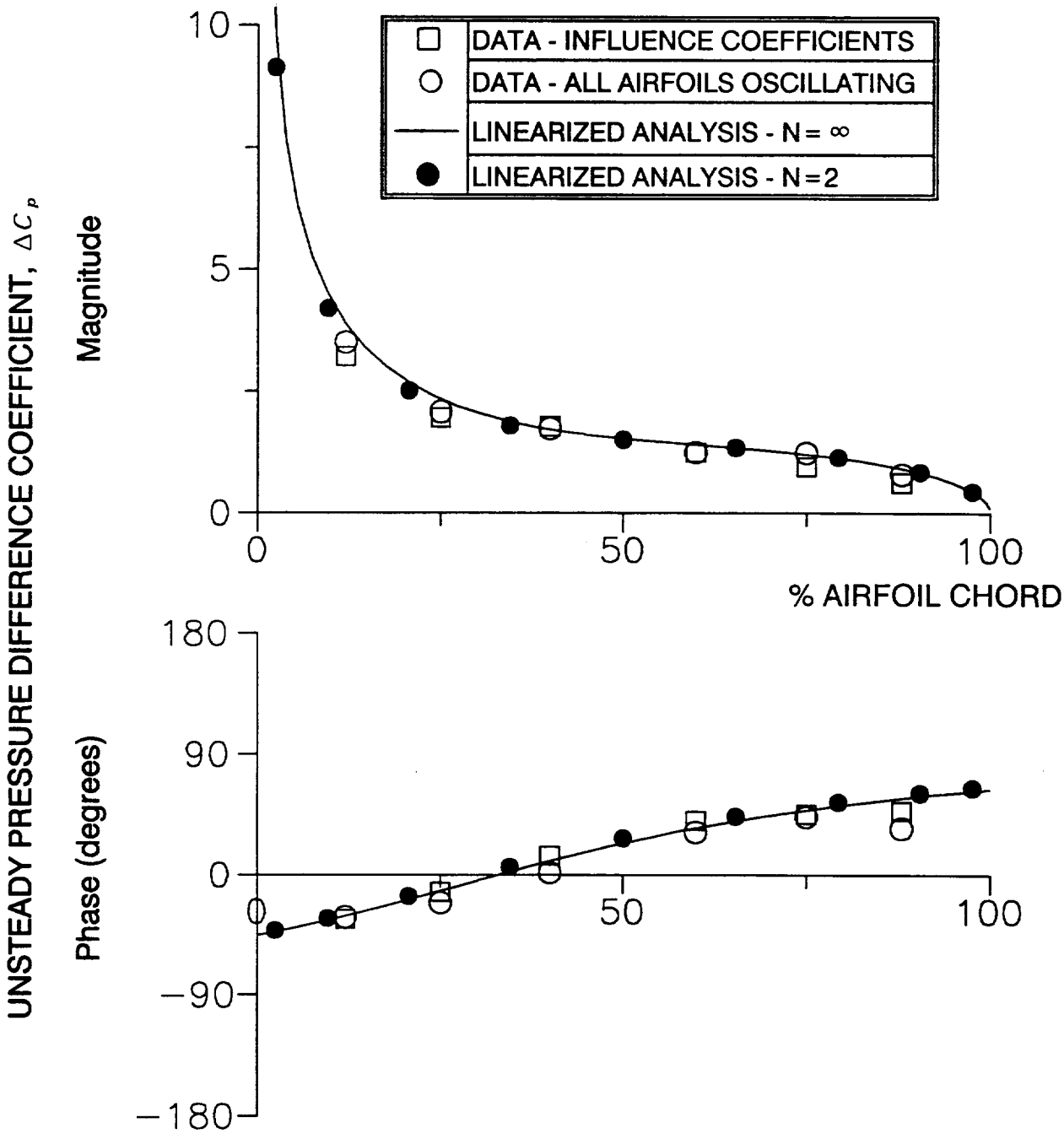

Figure 24 Unsteady pressure difference coefficient distribution, k=0.64, β =-90 degrees

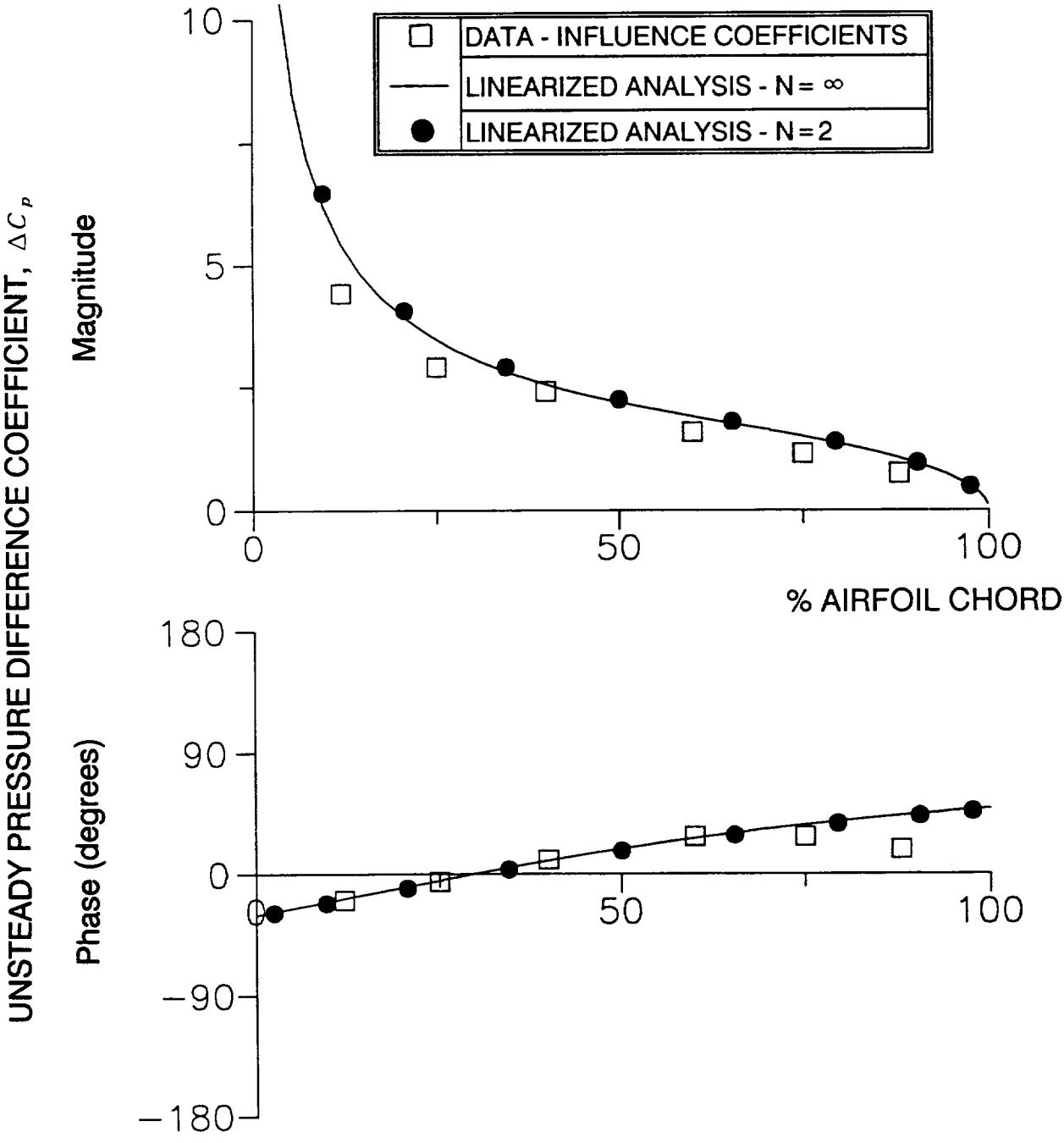

Figure 25 Unsteady pressure difference coefficient distribution, k = 0.64, β = 180 degrees

REPORT DOCUMENTATION PAGE

Form Approved
OMB No. 0704-0188

1. AGENCY USE ONLY (*Leave blank*)	2. REPORT DATE	3. REPORT TYPE AND DATES COVERED
	May 1993	Technical Memorandum

4. TITLE AND SUBTITLE

Effect of Wind Tunnel Acoustic Modes on Linear Oscillating Cascade Aerodynamics

5. FUNDING NUMBERS

WU-505-62-10

6. AUTHOR(S)

Daniel H. Buffum and Sanford Fleeter

7. PERFORMING ORGANIZATION NAME(S) AND ADDRESS(ES)

National Aeronautics and Space Administration
Lewis Research Center
Cleveland, Ohio 44135-3191

8. PERFORMING ORGANIZATION REPORT NUMBER

E-8171

9. SPONSORING/MONITORING AGENCY NAME(S) AND ADDRESS(ES)

National Aeronautics and Space Administration
Washington, D.C. 20546-0001

10. SPONSORING/MONITORING AGENCY REPORT NUMBER

NASA TM-106367

11. SUPPLEMENTARY NOTES

Prepared for the 38th ASME International Gas Turbine and Aeroengine Congress and Exposition sponsored by the American Society of Mechanical Engineers, Cincinnati, Ohio, May 24 -27, 1993. Daniel H. Buffum, Lewis Research Center and Sanford Fleeter, Thermal Sciences and Propulsion Center, School of Mechanical Engineering, Purdue University, West Lafayette, Indiana 47907. Responsible person, Daniel H. Buffum, (216) 433-3579.

12a. DISTRIBUTION/AVAILABILITY STATEMENT

Unclassified - Unlimited
Subject Category 07

12b. DISTRIBUTION CODE

13. ABSTRACT ***(Maximum 200 words)***

The aerodynamics of a biconvex airfoil cascade oscillating in torsion is investigated using the unsteady aerodynamic influence coefficient technique. For subsonic flow and reduced frequencies as large as 0.9, airfoil surface unsteady pressures resulting from oscillation of one of the airfoils are measured using flush-mounted high-frequency-response pressure transducers. The influence coefficient data are examined in detail and then used to predict the unsteady aerodynamics of a cascade oscillating at various interblade phase angles. These results are correlated with experimental data obtained in the traveling-wave mode of oscillation and linearized analysis predictions. It is found that the unsteady pressure disturbances created by an oscillating airfoil excite wind tunnel acoustic modes which have detrimental effects on the experimental data. Acoustic treatment is proposed to rectify this problem.

14. SUBJECT TERMS

Cascade; Unsteady aerodynamics

15. NUMBER OF PAGES

42

16. PRICE CODE

A03

17. SECURITY CLASSIFICATION OF REPORT	18. SECURITY CLASSIFICATION OF THIS PAGE	19. SECURITY CLASSIFICATION OF ABSTRACT	20. LIMITATION OF ABSTRACT
Unclassified	Unclassified	Unclassified	